Combined targeting of FAAH enzymes and melatonin receptors promotes neuroprotection and stimulates inflammation resolution

Journal:	*British Journal of Pharmacology*
Manuscript ID	2022-BJP-0520-RP
Manuscript Type:	Research Article
Date Submitted by the Author:	17-May-2022
Complete List of Authors:	Cammarota, Mariarosaria; University of Naples Federico II School of Medicine and Surgery Ferlenghi, Francesca; University of Parma Vacondio, Federica ; University of Parma de Rosa, Valeria; University of Naples Federico II School of Medicine and Surgery Vincenzi, Fabrizio; University of Ferrara Varani, Katia; University of Ferrara Bedini, Annalida; University of Urbino Department of Biomolecular Sciences Rivara, Silvia ; University of Parma Mor, Marco; University of Parma Boscia, Francesca; University of Naples Federico II School of Medicine and Surgery
Major area of pharmacology:	Neuropharmacology, Neurodegeneration/neuroprotection
Cross-cutting area:	Drug discovery/target validation, Inflammation
Additional area(s):	Cannabinoid, Glia

Combined targeting of FAAH enzymes and melatonin receptors promotes neuroprotection and stimulates inflammation resolution

[1]Mariarosaria Cammarota, [2]Francesca Ferlenghi, [2]Federica Vacondio, [1]Valeria de Rosa, [3]Fabrizio Vincenzi, [3]Katia Varani, [4]Annalida Bedini, [2]Silvia Rivara, [2]Marco Mor, [1]Francesca Boscia

[1]Division of Pharmacology, Department of Neuroscience, Reproductive Sciences and Dentistry, School of Medicine, Federico II University of Naples, Naples, Italy
[2] Department of Food and Drug, University of Parma, Parco Area delle Scienze 27/A, I-43124 Parma, Italy
[3]Department of Translational Medicine, University of Ferrara, 44121 Ferrara, Italy.
[4] Department of Biomolecular Sciences, University of Urbino "Carlo Bo", Piazza Rinascimento 6, I-61029 Urbino, Italy

Running title: Combined targeting FAAH enzymes and melatonin receptors promotes neuroprotection

***Correspondence**: Francesca Boscia PhD
Division of Pharmacology, Department of Neuroscience, Reproductive and Dentistry Sciences
School of Medicine, Federico II University of Naples
Via Sergio Pansini 5, 80131- Naples, Italy.
Tel: +39 81 7463326; Fax: +39 0817463323;
E-mail: boscia@unina.it

Number of figures: 9
Word count: 3838

Conflict of interest statement

None

Data availability statement

The data that support the findings of this study are available from the corresponding author upon reasonable request. Some data may not be made available because of privacy or ethical restrictions.

Acknowledgements

This work was financially supported by the Italian Ministry for University and Research (MIUR, PRIN 2017, 20175SA5JJ Project) to MM (Project Coordinator), and to FB (Research Unit Coordinator), and by the Programme "FIL-Quota Incentivante" of University of Parma and co-sponsored by Fondazione Cariparma to S.R. We also thank Dr Lucia D'Esposito for her invaluable support and Mrs Matilde Gallipari and Mr Luigi Di Guida for technical assistance.

Author Contributions

Conceptualization, FB; MM; Data curation, MC, FVa, SR, FVi, FB; Investigation, MC, FF, FVi, VdR, AB, FB; Formal analysis, MC, FVa, FVi, SR, FB; Writing – original draft FB, Writing – review & editing; MC, FV, KV, SR, MM; FB; Supervision, FB; Funding acquisition, MM, FB, SR. All authors have read and agreed to the final version of the manuscript.

Declaration of transparency and scientific rigour

This Declaration acknowledges that this paper adheres to the principles for transparent reporting and scientific rigour of preclinical research as stated in the BJP guidelines for Design and Analysis, Immunoblotting and Immunochemistry and Animal Experimentation, and as recommended by funding agencies, publishers and other organizations engaged with supporting research.

Abbreviations

ABCA1 ATP-binding cassette transporter number 1
AD Alzheimer's disease
AEA anandamide
ALS amyotrophic lateral sclerosis
AMPK adenosine 5′-monophosphate-activated protein kinase
BCA bicinchoninic acid
BSA bovine serum albumin
CB_1 cannabinoid receptor type 1
CB_2 cannabinoid receptor type 2
CNS Central Nervous System
DIV days in vitro
DMSO dimethyl sulfoxide
EC endocannabinoid
ECs endocannabinoids
EAE experimental autoimmune encephalomyelitis
FAAH fatty acid amide hydrolase
GFAP glial fibrillary acidic protein
GSH glutathione
GSSG glutathione disulphide
HBSS hank's balanced salt solution
HPLC-MS/MS high performance liquid chromatography coupled to tandem mass spectrometry
HS horse serum
IFN-γ interferon-γ
LPS lipopolysaccharide
LXR liver X receptor
MAP2 microtubule-associated protein 2
MBP myelin basic protein
MEL melatonin
MEM minimal essential medium
MS multiple sclerosis
MT1 melatonin receptor type 1
MT2 melatonin receptors type 2
NAEs N-acylethanolamines

NF200 neurofilament-200

NMDA N-Methyl-D-Aspartate

OEA N-oleoylethanolamine

PLIN2 perilipin2

PI propidium iodide

PEA N-palmitoylethanolamine

PPARα peroxisome proliferator-activated alpha receptor

SFM serum-free medium

TNFα tumor necrosis factor-alpha

TREM2 triggering receptor expressed on myeloid cells-2

TRPV1 transient receptor potential vanilloid 1

BULLET POINT

What is already known

- Enhancing the endocannabinoid and melatonergic tone has therapeutic potential to treat neuroinflammatory diseases

- UCM1341 is a dual-acting-compound with FAAH inhibitory action and agonistic activity on melatonin receptors

What this study adds

- UCM1341 exhibits neuroprotection against neuroinflammatory degeneration and stimulates inflammation resolution pathways

- The activation of PPARα, TRPV1 and melatonin receptors contributes to UCM1341 beneficial effects

What is the clinical significance

- FAAH inhibition and the activation of melatonin receptors represent a synergistic drug combination to provide neuroprotection against the neuroinflammatory damage

- Our findings provide an encouraging prospect of therapeutically targeting EC and melatonergic systems in CNS inflammatory demyelinating states.

Abstract

Background and Purpose

Deciphering novel strategies to therapeutically foster inflammation resolution and neuroprotection is an unmet clinical need. Enhancing the endocannabinoid (EC) tone by inhibiting the catabolic enzyme FAAH or stimulating melatonin receptors have therapeutic potential to treat neuropathological states in which neuroinflammation play a central role.

Experimental Approach

By employing a rodent hippocampal explant model of inflammatory injury we reveal the effects of UCM1341, a dual-acting compound with FAAH inhibitory action and agonistic activity on melatonin receptors, against the neuroinflammatory damage. FAAH activity was measured by a radiometric assay and N-acylethanolamine levels were assessed by HPLC-MS/MS. FAAH distribution, evolution of inflammation and the contribution of UCM1341 to the expression of proteins controlling macrophage behavior were investigated by biochemical and confocal analyses.

Key Results

UCM1341 exhibited greater neuroprotection against neuroinflammatory degeneration if compared to the reference compounds URB597 (FAAH inhibitor) or melatonin. During neuroinflammation, UCM1341 augmented the levels of AEA and OEA, but not PEA, upregulated PPARα receptor levels, attenuated demyelination, and prevented the release of TNFα. The bivalent ligand modulated the inflammatory response by contributing to microglia/macrophage polarization, stimulating the formation of lipid-laden macrophages, and regulating the expression of proteins controlling cholesterol metabolism and efflux. The neuroprotective effects of UCM1341 were prevented by PPARα, TRPV1 and melatonin receptor antagonists.

Conclusions and Implications

UCM1341**,** by enhancing the EC and melatonergic signalling, benefits neuroprotection and stimulates inflammation resolution pathways. Our findings provide an encouraging prospect of therapeutically targeting EC and melatonergic systems in CNS inflammatory demyelinating states.

Keywords: neuroinflammation, endocannabinoid system, FAAH, melatonin, AEA, OEA, PPARα, TRPV1 N-acylethanolamines, URB597.

Introduction

Neuroinflammation is a critical determinant for the pathogenesis of several neurodegenerative disorders and chronically contributes to glia dysfunction, neuronal death and remyelination failure in multiple sclerosis (MS) or Alzheimer's disease (AD) (Franklin and Ffrench-Constant, 2017). Promoting neuroprotection and modulating the microglia/macrophage response are important therapeutic goals to accelerate myelin repair, improve functional recovery and prevent disease progression (Boscia et al., 2021).

Enhancing the endocannabinoid (EC) signalling and stimulating the melatonergic system may represent a therapeutic strategy in neuroinflammatory and neurodegenerative conditions such as MS and AD (Chiurchiu et al., 2018; Reiter et al. 2013). Nevertheless, a combination of the two approaches has not been investigated.

Endocannabinoids (ECs) are lipid mediators released on demand from membrane phospholipid precursors, exerting their effects *via* the activation of cannabinoid CB_1/CB_2 receptors and non-cannabinoid receptors, including peroxisome proliferator-activated receptors (PPARs), transient receptor potential vanilloid type-1 (TRPV1), and other G-protein-coupled receptors. Inhibition of the EC-hydrolysing enzyme fatty acid amide hydrolase (FAAH) increases the levels of biologically active EC lipids and related ethanolamides, including anandamide (AEA), N-oleoylethanolamine (OEA), and N-palmitoylethanolamine (PEA). While AEA is an endocannabinoid substance, the other ethanolamides exert their activity through different targets, sustaining the immunomodulatory and neuroprotective activity (Piomelli, 2003; Petrosino and Di Marzo, 2010). The pharmacological inhibition of FAAH is considered a valuable therapeutic approach to treat anxiety and depression disorders, and to enhance antinociceptive and anti-inflammatory effects, and provide neuroprotection (van Egmond et al., 2021).

The indoleamine melatonin (N-acetyl-5-methoxytryptamine), the main neurohormone of pineal glands, regulates many physiological functions acting via non-receptor and receptor-dependent signalling pathways and is provided by immunomodulatory and protective roles. Even if the cytoprotective effect of melatonin has been often related to its direct antioxidant mechanism, increasing evidence highlights an important role of its receptor activity (Kopustinskiene and Bernatoniene, 2021).

Recently, our research group developed dual-acting compounds, with potent and balanced FAAH inhibitory action and agonistic activity on melatonin receptors (Spadoni et al., 2018). Among them, UCM1341, having nanomolar MT1/MT2 binding affinity and inhibitory potency on FAAH, was able to reduce intraocular pressure, an effect exerted by both melatonin and cannabinoid substances, showing improved activity compared to single agents.

In the present study, we investigated whether FAAH inhibition combined with the activation of melatonin receptors may represent a synergistic drug combination to provide neuroprotection.

To this aim, we tested the effects of UCM1341 and the reference compounds, melatonin and URB597 (FAAH inhibitor), alone or in combination, against N-Methyl-D-Aspartate (NMDA)-induced excitotoxicity or lipopolysaccharide (LPS)+interferon-γ (IFN-γ)-induced neuroinflammatory damage in rat hippocampal explant cultures. UCM1341 exerted a greater neuroprotection against the neuroinflammatory insult if compared to the reference compounds melatonin or URB597. Under neuroinflammatory conditions, UCM1341 upregulated PPARα receptor levels, augmented AEA and OEA levels, attenuated demyelination, and prevented TNFα release. The bivalent ligand modulated the inflammatory response by contributing to microglia/macrophage polarization, stimulating the formation of lipid-laden macrophages, and regulating the expression of proteins controlling cholesterol metabolism and efflux. The neuroprotective effects of UCM1341 were prevented by the PPARα, TRPV1 and the melatonin receptor antagonists, revealing the synergistic contribution of both ECs and melatonergic signalling to the beneficial effects of the bivalent ligand during neuroinflammation.

Material and Methods

Chemicals

[1,1'-biphenyl]-3-yl (6-((3-(2-acetamidoethyl)-2-bromo-1*H*-indol-5-yl)oxy)hexyl)carbamate) (UCM1341) was synthesized according to the procedure described in literature (Spadoni et al., 2018). Cyclohexylcarbamic acid 3'-(aminocarbonyl)-[1,1'-biphenyl]-3-yl ester (URB597), N-acetyl-5-methoxytryptamine (melatonin), propidium iodide (PI), NMDA, LPS, recombinant human INF-γ were from Merck-Life Science. All media and serum for organotypic cultures were purchased from Gibco (Thermo Fisher Scientific, Inc). UCM1341, URB597, melatonin, 1-(2,4-dichlorophenyl)-5-(4-iodophenyl)-4-methyl-N1-piperidinyl-1*H*-pyrazole-3-carboxamide (AM251), [6-iodo-2-methyl-1-[2-(4-morpholinyl)ethyl]-1*H*-indol-3-yl](4-methoxyphenyl)-methanone (AM630), (3-(4-chlorophenyl)-N-(3-methoxyphenyl)-2-propenamide) (SB366791), and (N-[2-[2-(phenylmethyl)-1*H*-indol-3-yl]ethyl]-acetamide (luzindole) were dissolved in dimethylsulfoxide (DMSO; stock solutions of 25 mM), aliquoted and kept frozen at -20°C. NMDA was dissolved in serum-free medium (stock solution of 10 mM); LPS was dissolved in pyrogen-free water, and IFN–γ in Dulbecco's phosphate-buffered saline containing 0.1% bovine serum albumin (BSA). Stock solutions were diluted to achieve the desired drug concentration immediately before use. Maximal DMSO concentration was ≤0.1%; this concentration did not affect cell viability in organotypic cultures (Boscia et al., 2006).

For analytical determinations, the standards for AEA, OEA, PEA, and their corresponding deuterated (d4) internal standards were supplied by Cayman Chemicals (Ann Arbor, MI, USA) as stock solutions in ethanol. Reduced glutathione (GSH) and glutathione disulphide (GSSG) were purchased from Sigma-Aldrich (Sigma-Aldrich srl, Milan, Italy) as powders. HPLC grade acetonitrile and formic acid were supplied by VWR International (VWR International, Milan, Italy). [^{3}H]-AEA (specific activity: 60 Ci/mmol), employed as a substrate for *in vitro* FAAH activity assay, was supplied by American Radiolabeled Chemicals (St. Louis, MI, USA). All other chemicals not mentioned otherwise were from Merck-Life Science.

Animals

All animal experiments and animal handling and care were in accordance with the ARRIVE guidelines and the Guide for the Care and Use of Laboratory Animals (EU Directive 2010/63/EU), and the experimental protocol was approved by the Animal Care and Use Committee of "Federico II" University of Naples, Italy, and Ministry of Health, Italy (#515/2019-PR). Female Wistar rats (14-days timed pregnant) were obtained from Charles River Laboratories (Italy) and maintained at a constant temperature (22 -1°C) on a 12-h light/dark cycle (lights on at 7 AM) with food and water *ad*

libitum. The pregnant dams were allowed to deliver their pups naturally; 7-9 days postpartum littermates were used for the preparation of organotypic explants. All efforts were made to minimize animal suffering and to reduce the number of animals used.

Hippocampal organotypic explants

Organotypic explants prepared as previously described (Boscia et al., 2006; 2008). Briefly, 400µm-thick parasagittal slices were obtained from hippocampi of P7- to P9-day-old Wistar rat pups (Charles River Laboratories, Calco, Italy) using a McIlwain tissue chopper (Campden Instruments, Leicester, UK) and placed into ice-cold Hank's balanced salt solution (HBSS, Gibco, Italy) supplemented with 5 mg/ml glucose and 1.5% (v/v) fungizone. Cultures were then transferred to a humidified semiporous membrane (30mm Millicell tissue culture plate inserts of 0.4 mm pore size from Millipore, Italy) in six-well tissue culture plates (5 slices per membrane). Each well contained 1.2 ml of tissue culture medium consisting of 50% minimal essential medium (MEM, Gibco, Monza, Italy), 25% HBSS, 25% heat inactivated horse serum (HS), 6.5 mg/ml glucose, 1 mM glutamine, and 1.5% fungizone (normal medium). Cultures were maintained at a 37°C and 5% CO_2-conditioned atmosphere. Experiments were performed on cultures kept *in vitro* for 7 days (7 DIV) or 10 days (10 DIV).

LPS plus INF-γ-induced neurodegeneration and drug exposure

Hippocampal explants were removed from normal serum-containing medium, washed in serum-free medium (SFM) (consisting of normal medium with serum replaced with MEM, plus 1% HS) and exposed to a combined application of 10µg/ml LPS plus 100ng/ml INF–γ for 72-96 hours in SFM. This model, by mimicking the microglia interaction with infiltrating peripheral immune T cells, triggers the release of massive proinflammatory and cytotoxic factors, and promotes an inflammatory neurodegeneration (Papageorgiou et al., 2010). Appropriate concentrations of UCM1341 (0.1-10µM), URB597, (10µM), melatonin (10µM), or vehicle (DMSO ≤0.1%) were added to the medium at the beginning of the insult, and were kept in the culture medium during the entire duration of the experiment. Luzindole (0.1-10µM), AM251 (0.1-10µM), AM630 (0.1-10µM), SB3667 (0.03-10µM); GM6471 (10µM) were preincubated for 1 hour before the insult and used at concentrations that displayed no effect when used alone (Landucci et al., 2021). Control culture explants were kept in SFM, in the absence or in the presence of testing compounds.

NMDA-induced neurodegeneration and drugs exposure

NMDA exposure was performed in hippocampal cultures as previously described (Boscia et al., 2006). Organotypic hippocampal slice cultures were removed from NM, washed in SFM and exposed to 10-30μM NMDA (with or with-out testing compounds) for 48 hours in fresh SFM. Control hippocampal cultures were kept in SFM.

Assessment of cell death and image analysis

Cell injury was assessed in explants by live incorporation of a marker of compromised membrane integrity, propidium iodide (PI, 5 μg/ml, Molecular Probes), that emits a bright red fluorescence when exposed to blue-green light. For densitometric measurements, the digital pictures were analyzed with the Image Pro-Plus software (Media Cybernetics), after freehand outlining of the CA neuronal layer, as previously described (Boscia et al., 2006, 2008).

Immunoblotting

Explant extract preparation and immunoblotting were performed as previously described (Boscia et al., 2015). The slices were lysed in 50 mM Tris-HCl pH 8.0 buffer containing 150 mM NaCl, 1% Nonidet P-40, 2 μg/ml aprotinin, 1 μg/ml pepstatin, 2 μg/ml leupeptin, 1 mM Na3VO4. Protein concentration was determined by the Bradford assay using bovine serum albumin (BSA) as the standard and the crude extracts were subjected to 8 or 14% sodium dodecyl sulphate polyacrylamide gel. Then, gels were electrophoretically transferred onto nitrocellulose membranes and filters were probed with the indicated primary antibodies: polyclonal anti-FAAH (1:5000, Cayman, RRID:AB_327842) polyclonal anti-glial fibrillary acidic protein GFAP (1:1000, Sigma, RRID:AB_476889), monoclonal anti-Iba1 (1:2000, Dako), monoclonal anti-MEL-1A/B-R (1:1000, Santa Cruz, RRID:AB_2833090) monoclonal anti-myelin basic protein (MBP, 1:1000, Merck, RRID:AB_240845), polyclonal anti-mannose receptor CD206 (1:5000, Abcam, RRID:AB_10896526), polyclonal anti- adenosine 5′-monophosphate-activated protein kinase (AMPK) and anti-phospho-AMPK, (1:1000, each, Cell Signaling, RRID:AB_310416, RRID:AB_390759), monoclonal anti-triggering receptor expressed on myeloid cells-2 (TREM2, 1: 1500, Santa Cruz, RRID:AB_1130660), monoclonal anti-liver X receptor 1:300 (LXR, Santa Cruz, RRID:AB_2251583), monoclonal anti-ATP binding cassette transporter number 1 (ABCA1; 1:1000, Santa Cruz, RRID:AB_830977), monoclonal anti-PPARα (1:600, Santa Cruz, RRID:AB_2165759); anti-β–actin (1:1000, Sigma, RRID:AB_476744). Proteins were visualized with peroxidase-conjugated secondary antibodies, using the enhanced chemiluminescence system (Amersham-Pharmacia Biosciences LTD, Uppsala, Sweden). Films were scanned and the signal ratio protein of

interest/housekeeping protein was quantified densitometrically. Where indicated, filters have been stripped as described (Cammarota et al., 2021). The immuno-related procedures used comply with the recommendations made by the British Journal of Pharmacology.

Confocal microscopy

Confocal immunofluorescence procedures in organotypic explants were performed as previously described (Boscia et al., 2013; de Rosa et al., 2019). Slices were fixed in 4% wt/vol. paraformaldehyde in phosphate buffer (PB) for 1 hour, blocked with 3% BSA and 0.05% Triton X (Sigma) for 40 minutes, and then incubated with the following primary antibodies: rabbit polyclonal anti-FAAH (1:1500, Cayman), polyclonal anti-GFAP (1:1000, Sigma, RRID:AB_476889), polyclonal anti-Iba1 (1:2000, Wako #19-19741), monoclonal anti-CD11b (Thermo Fisher Scientific, Inc., RRID:AB_2536484), monoclonal anti-microtubule-associated proteins MAP2 (1:2000, Millipore, RRID:AB_91939), polyclonal anti- neurofilament-200 (anti-NF200; 1:500, Sigma, RRID:AB_1842647), monoclonal anti-MBP (1:1000, Millipore #MAB386), polyclonal anti- CD206 (1:13000, Abcam, RRID:AB_10896526), polyclonal anti-GABA (1:400, Merk, RRID:AB_213533), polyclonal anti-perilipin2 (Plin2; 1:3000, Progen, RRID:AB_2895086), monoclonal anti-ABCA1 (1:400, Santa Cruz, RRID:AB_830977). After 48 hours at 4°C, slices were incubated with the corresponding secondary antibodies for two hours at room temperature. Finally, they were mounted on glass slides and imaged with Zeiss LSM 700 laser (Carl Zeiss) scanning confocal microscope.
Controls of the methods included replacement of the primary antisera with normal serum (1:200). To control for a possible cross-reactivity between IgGs in double immunolabeling experiments, some sections were processed through the same immunocytochemical sequence except that primary antisera were replaced with normal serum, or only one primary antibody was applied, but the full complement of secondary antibodies was maintained. In addition, the secondary antibodies utilized were highly pre-adsorbed to the IgGs of numerous species. Tissue labeling without primary antibodies was also tested to exclude autofluorescence. No specific staining was observed under these control conditions, thus confirming the specificity of the immunosignals.

Quantification of confocal studies in hippocampal explants

Confocal microscopy was used to obtain stacks of photographs of FAAH/MAP2, FAAH/GFAP, FAAH/CD11b and MBP/NF200 immunolabeling at 2-µm intervals in CA1 area at ×40 magnification and a resolution of 1,024 × 1,024, between a depth of 5–20 µm from the upper surface. Four slices were analyzed per condition in each experimental sessions. Five images of randomly chosen areas of each slice were acquired with identical fluorescence intensity. Maximum intensity projection (MIP) images were created for each stack by using ZEN imaging software. Then, for each MIP image the

quantification of co-localization between FAAH MAP2, FAAH and GFAP, FAAH and CD11b, and MBP with NF200 immunostaining was assessed by using the 'co-localization highlighter' plug-in for the ImageJ software (NIH, Bethesda, MA, USA) (de Rosa et al., 2019). Before co-localization analysis, images were first thresholded to identify the positive signal, subsequently, the pixels expressing both FAAH and MAP2, GFAP and Iba1 and MBP, NF200 were identified. Finally, the number of pixels positive for FAAH/MAP, FAAH/GFAP, FAAH/CD11b, and MBP/NF200 was measured per microscope field. This value, expressed as percentage of co-localization, represents the extent of FAAH/MAP2, FAAH/GFAP, FAAH/CD11b and MBP/NF200 coexpression.

Quantification of immunofluorescence intensities were quantified in terms of pixel intensity by using the NIH image software, as described previously (Casamassa et al., 2016). Digital images were taken with 40 × objective and identical laser power settings and exposure times were applied to all the photographs from each experimental set.

The number of GABA- and CD206-positive cells as well as double-labelled $Iba1^{+}/Plin2^{+}$ cells was determined in the CA1 region by manual counting at × 40 magnification. Only cells with clearly a visible cell body and profiles were counted.

Microglia cell morphology in the CA1 region was evaluated with Iba1 immunostaining (Boscia et al., 2009). Individual $Iba1^{+}$ cells were scored according to their morphology in 4 main categories: (i) *resting and intermediate*, including microglia characterized by small cell bodies and radial thin processes (resting) or larger/elonged cell body and shorter thick processes (intermediate), (ii) *amoeboid*, including spherical cells with or without very short processes (*iii*) *foamy,* having a vacuolated bubbly cytoplasm, and (*iv*) *dystrophic*, characterized by twisted and fragmented processes

Quantification of cell surface area occupied by GFAP protein was performed with ImageJ using the application: threshold from background, followed by manually defining the area, and finally measuring the area fraction above the threshold.

IL-6, IL-10 and TNFα quantification

IL-6 and L-10 levels were measured by using specific AlphaLISA detection kits (Perkin Elmer Life and Analytical Sciences, Boston, MA, USA). Briefly, aliquots of the samples were incubated in presence of biotinylated anti-analyte antibody and anti-analyte antibody-conjugated acceptor beads. After 60 min incubation, streptavidin-coated donor beads were added. Upon excitation at 680 nm, a photosensitizer inside the donor beads converts ambient oxygen to an excited singlet state that produces a chemiluminescent reaction in the acceptor beads. The resulting light emission, proportional to the amount of analyte, was read at 615 nm with a Perkin Elmer EnSight Multimode Plate Reader.

TNFα levels were determined with a quantitative sandwich ELISA kit (Elabsciences, Houston, TX, USA) following manufacturer instructions. The reaction was developed with streptavidin-horseradish peroxidase and the optical density was measured spectrophotometrically at a wavelength of 450 nm in a Perkin Elmer EnSight Multimode Plate Reader (Vincenzi et al., 2017). Experiments were performed in duplicate.

Quantification of N-acylethanolamines (NAEs) in hippocampal cultures

Fatty acid ethanolamides AEA, OEA and PEA were extracted from hippocampal tissue homogenates by protein precipitation via acetonitrile addition, as previously reported (Carnevali et al., 2020) Briefly, 100 µm thick hippocampal tissue slices (5 slices) were homogenized in 100 µl of TRIS buffer (50 mM, pH 7.5, 4°C) containing 0.32 M sucrose. Two volumes of acetonitrile, containing 100 nM AEA-d4, OEA-d4 and PEA-d4 as internal standards, were added, and, after centrifugation (16000 g, 10 min, 4°C), levels of NAEs were quantified by high performance liquid chromatography coupled to tandem mass spectrometry (HPLC-MS/MS). Compound-dependent parameters were optimized by flow injection analysis of 5 µM standard solutions in methanol. Acquisition occurred in positive ion (ESI+) and in multiple reaction monitoring (MRM) mode. For quantitative analysis, the following parent-product ions transitions were selected: AEA: m/z 348.2 $[M+H]^+ \rightarrow$ m/z 90.9 + m/z 62.1 Tube Lens (TL): 54 V; Collision Energy (CE): 42; 14 eV, respectively; AEA-d4: m/z 352.2 $[M+H]^+ \rightarrow$ m/z 202.8 + m/z 66.3 (TL: 76 V; CE: 12; 17 eV); OEA: m/z 326.3 $[M+H]^+ \rightarrow$ m/z 309.3 + m/z 93.3 + m/z 62.3 (TL: 115 V; CE: 10; 19; 28 eV); OEA-d4: m/z 330.1 $[M+H]^+ \rightarrow$ m/z 313.4 + m/z 66.2 (TL: 67 V; CE: 14; 15 eV); PEA: m/z 300.3 $[M+H]^+ \rightarrow$ m/z 62.3 (TL: 54 V; CE: 14; 42 eV); PEA-d4: m/z 304.2 $[M+H]^+ \rightarrow$ m/z 287.1 + m/z 66.3 (TL: 72 V; CE: 12; 15 eV). A Waters XSelect HSS T3 column (Waters Corp, USA, 100 x 2.1 mm, 3.5 µm particle size) was employed for gradient separation. Eluent A: acetonitrile + 0.1% v/v formic acid; eluent B: water + 0.1% v/v formic acid. t(0 min): 5%A:95%B; t(1 min): 5%A:95%B; t(6 min): 100%A:0%B; t(11 min): 100%A:0%B; t(12 min): 5%A:95%B, with a 3-min equilibration time; total run time: 15 min. Solvent flow was 0.22 mL/min. Injected volume: 10 µl. Calibration curves were prepared in the 0.5-500 nM concentration range for AEA and in the 2.5-500 nM range for OEA and PEA, by spiking 2 µl of a DMSO stock solution containing the compound mixture in 198 µl of charcoal treated rat plasma and processing the calibration standards following the same procedure described for unknown samples. Calibration curves showed good linearity with coefficients of correlation (r2) > 0.99. The limit of quantification (LOQ) was equal to 0.5 nM for AEA, 2.5 nM for OEA and PEA. Total protein content in hippocampal tissue homogenates was quantified by the bicinchoninic acid (BCA) protein kit (Pierce

Biotechnology, Rockford, IL, USA) following supplier's protocol and NAEs content was expressed as pmol/mg protein.

Determination of glutathione (GSH) and glutathione disulfide (GSSG) levels in hippocampal cultures

Reduced GSH and GSSG were measured by HPLC-MS/MS starting from hippocampal tissue homogenates obtained according to the procedure described in the previous paragraph. Briefly, two volumes of acetonitrile containing 0.1% HCOOH were added to one volume of hippocampal tissue homogenate. After centrifugation (16000 g, 10 min, 4°C), levels of GSH and GSSG were quantified by HPLC-MS/MS. A Waters XSelect HSS T3 column (Waters Corp, USA, 100 x 2.1 mm, 3.5 µm particle size) was employed for gradient separation. Eluent A: acetonitrile + 0.1% v/v formic acid; eluent B: water + 0.1% v/v formic acid. Gradient conditions: t(0 min): 5%A:95%B; t(3 min): 5%A:95%B; t(4 min): 100%A:0%B; t(5 min): 100%A:0%B; t(5.5 min): 5%A:95%B, with a 2.5-min equilibration time; total run time: 8 min. Solvent flow was 0.22 ml/min. Injected volume: 10 µl. For quantitative analysis, the following parent-product ions transitions were selected: GSH m/z 308.0 $[M+H]+\rightarrow$ m/z 162.0 + m/z 84.2 + m/z 76.2 TL: 106 V; CE: 14, 23, 28 eV; GSSG m/z 613.1 $[M+H]+\rightarrow$ m/z 484.1 + m/z 354.9 + m/z 230.9 TL: 138 V; CE: 17, 21, 33 eV. Calibration curves showed good linearity in the 100 nM-20 mM concentration range for both GSH and GSSG. GSH levels were expressed as nmol/mg protein.

HPLC/MS/MS system configuration

A Thermo Accela UHPLC gradient system coupled to a Thermo TSQ Quantum Max triple quadrupole mass spectrometer (Thermo, USA) equipped with a heated electrospray ionization (H-ESI) ion source was employed for NAEs, GSH and GSSG quantification. H-ESI source tune parameters were set as follows: probe middle (D) position; capillary temperature: 270°C; spray voltage: 4.0 kV. Nitrogen was used as nebulizing gas at the following pressure: sheath gas: 35 psi; auxiliary gas: 15 arbitrary units (a.u.). Argon was used as collision gas at a pressure of approximately 1.5 mtorr (1 torr = 133.3 Pa). The software Xcalibur version 2.2 (Thermo, USA) was employed for HPLC/MS/MS data acquisition and processing.

FAAH activity assay

Previously obtained hippocampal tissue homogenates underwent centrifugation (1000 g, 10 min, 4 °C) and total protein content was quantified in the supernatant by the BCA protein kit. FAAH activity was measured in the samples by incubating 50 µg of protein from hippocampal homogenates with

[^{3}H]-AEA (10,000 dpm) and 10 μM AEA for 30 min at 37 °C in 0.5 mL TRIS buffer (50 mM, pH 7.5) containing fatty acid-free BSA (0.05%, w/v), as previously reported (Clapper et al., 2009) Enzymatic reaction was quenched by addition of 1 ml of 1:1 chloroform:methanol mixture. After centrifugation (2000 g, 10 min, 4°C), [^{3}H]-ethanolamine was measured in the aqueous phase by liquid scintillation counting.

Data and statistical analysis

The data and statistical analysis comply with the recommendations of the British Journal of Pharmacology on experimental design and analysis in pharmacology (Curtis et al., 2018). All the experiments were designed to generate groups of equal size, using randomization. Sample size and number of replicates are indicated in the figure legends. Group size is the number of independent values and statistical analysis was undertaken only for studies where each group size was at least n=5. Sample processing and quantification in microscopy studies were performed in a blinded manner. For pharmacological treatments, the investigator was not blinded to the experimental groups. In some experiments, data were normalized to reduce unwanted sources of variation. The data are expressed as the mean ± SEM of the values obtained from individual experiments. Statistical comparisons between two groups were performed by two-tailed Student's t-test (for parametric data and Gaussian distribution). Statistical comparisons for multiple groups were performed by one-way analysis of variance (ANOVA) followed by Bonferroni, post hoc test. GraphPad Prism 6.0 was used for statistical analysis (GraphPad Software, Inc, La Jolla, CA, USA). Post hoc tests were conducted only if F in ANOVA achieved $p < 0.05$ and there was no significant variance in homogeneity. *$p< 0.05$ was considered the threshold for statistical significance.

Nomenclature and targets and ligands

Key protein and targets and ligands in this article are hyperlinked to corresponding entries in http://www.guidetopharmacology.org and are permanently archived in the Concise Guide to Pharmacology 2021/2022.

Results

Neuroprotective effects of UCM1341 against NMDA-induced excitotoxicity in organotypic hippocampal explants

To study the neuroprotective potential of the bivalent ligand UCM1341, we investigated the effects of 0.1-10 μM UCM1341 against a milder and more severe excitotoxic insult induced by 10 or 30 μM NMDA exposure (Boscia et al., 2006). When hippocampal explants were exposed to 10 μM NMDA for 48 hours, cell death selectively occurred in the CA1 pyramidal cell layer and, to a lesser degree, in the CA3. By contrast, higher concentrations of 30 μM NMDA caused more marked neurodegenerative effects that involved both CA1 and CA3 (Figures 1A-B). When slices were incubated with 10 μM NMDA, a significant prevention of PI uptake in the CA1 region was observed with 1-10 μM UCM1341 (about 30%). Conversely, the bivalent ligand was less effective in counteracting CA degeneration induced by 30 μM NMDA, and a significant neuroprotective effect was observed only with 10 μM UCM1341 (Figure 1B).

Then, we investigated the synergistic neuroprotective potential of reference compounds, melatonin and URB597, against NMDA-induced neurodegeneration. To this aim, hippocampal explants were exposed to 10 μM NMDA, in the absence or presence of melatonin or URB597, alone or in combination. As shown in Figure 1C, 10 μM melatonin, but not 10 μM URB597, exerted a significant neuroprotection in the CA1 against NMDA-induced excitotoxicity (about 35%). When melatonin and URB597 were applied in combination (both at 10 μM), a significant neuroprotection was observed in the CA1 region, an effect that was comparable to that of both melatonin and UCM1341 (Figure 1C). Drug treatments in control slices did not affect cell viability at any of the concentrations used or time points analyzed, as revealed by PI uptake (data not shown).

LPS+IFN-γ exposure preferentially induced inflammatory degeneration in the CA1 region and modulated FAAH enzymes and melatonin receptors expression in brain cells

Next, to study the neuroprotective potential of UCM1341 on neuroinflammatory damage, hippocampal slice cultures were exposed to a combined application of 10 μg/ml LPS and recombinant 100 ng/ml IFN-γ for 3-4 days. We show that the cell degeneration, which abruptly appeared after 72 (in 7 DIV slices) or 96 hours (in 10 DIV slices) of LPS+INF-γ exposure can be monitored by PI uptake in hippocampal explant cultures (Figure 2A-B). Quantitative densitometric analysis showed that when the insult was applied to hippocampal slice cultures at 7 DIV, a significant upregulation of PI uptake in the CA1 region was recorded after 72 hours, while the CA3 and DG subregions were less affected (Figure 2A). When 10 DIV hippocampal cultures were exposed to LPS+INF-γ, PI uptake

significantly and selectively increased in the CA1 region after 96 hours (Figure 2B). The pro-inflammatory insult significantly upregulated the protein levels of the microglial Iba1 marker after 48 hours of LPS+IFN-γ exposure (Figure 2C-D), and induced demyelination, as revealed by the significant reduction of MBP levels (Figures 2F, H) and MBP immunoreactivity after 72 hours (Figure 2I). Next, we investigated the impact of the inflammatory insult on melatonin receptors and endocannabinoid hydrolyzing FAAH enzyme expression. As shown in Figure 2C, the non-selective anti-MT1/MT2 receptor antibody revealed that both MT1 and MT2 levels concomitantly increased 48 hours after the insult. MT2 proteins also increased after 24 hours, while MT1/MT2 levels significantly decreased after 72 hours (Figure 2C and E).

In line with previous studies (Gulyas et al., 2004), confocal analysis performed with anti-FAAH antibodies in hippocampal explants showed the predominant distribution of FAAH enzyme in somata and dendrites of principal cells (Figure 3A-C). Quantitative confocal analysis in the CA1 region revealed that the fluorescence intensity of both FAAH and GFAP, but not of MAP2 and the microglial marker CD11b, significantly increased 24 hours after LPS+IFN-γ exposure if compared to untreated controls (Figure 3A-B, E). At this latter time point, coexpression studies showed a significant increase of FAAH expression in MAP^+ neurons and $GFAP^+$ astrocytes (Figure 3A-B, F). After 48 hours, FAAH immunofluorescence returned to basal level, while GFAP and CD11b immunofluorescences were significantly upregulated (Figure 3C-D, G). Nevertheless, quantitative confocal analysis revealed a significant increased coexpression of FAAH with $CD11b^+$ microglia and $GFAP^+$ astrocytes, but not with MAP^+ neurons (Figure 3C-D, H).

UCM1341 attenuated LPS+IFN-γ induced demyelination, GABAergic interneurons loss and exerted a greater neuroprotection against the neuroinflammatory insult if compared to the reference compounds melatonin and URB597

To investigate the effects of UCM1341 on inflammation-mediated neurodegeneration, 10 DIV slices were exposed to 10 μg/ml LPS + 100 ng/ml IFN-γ in the absence or in the presence of 0-1-10μM UCM1314 for 4 days. Densitometric analysis of PI uptake revealed that UCM1341 exerted a marked and dose-dependent neuroprotective actions in the more vulnerable CA1 region (Figure 4A). At 10 μM, UCM1341 counteracted cell death occurring after LPS + IFN-γ exposure (Figure 4A, e).

To explore the synergistic neuroprotective potential of reference compounds, hippocampal explants were exposed to LPS+IFN-γ in the absence or in the presence of 10 μM melatonin or 10 μM URB597, alone or in combination. Both melatonin and URB597 exerted a significant neuroprotection against LPS+IFN-γ- induced neurodegeneration (about 30 %), as recorded by PI uptake after 96 hours. When drugs were used in combination (both at 10 μM), they fully counteracted cell death in the CA1 region,

thus demonstrating the synergistic neuroprotective effect of melatonin and URB597 against LPS+IFN-γ-induced inflammatory damage (Figure 4B, e).

Next, to explore the protective effects of UCM1341 on myelin and neurons during LPS+IFN-γ exposure, hippocampal explants were analyzed for MBP/NF200 colocalization and GABA distribution by confocal analysis. As shown in Figure 4, UCM1341 significantly prevented the loss of NF200 immunoreactivity (Figure 4C, m), and inhibitory $GABA^+$ interneurons in the CA1 region (Figure 4D). Moreover, the drug treatment attenuated axonal demyelination induced by LPS+IFN-γ-exposure, as indicated by the quantification of the myelination index 96 hours after the insult (Figure 4C, n).

UCM1341 inhibited FAAH activity and enhanced AEA and OEA in hippocampal explants during the neuroinflammatory injury

To investigate the mechanism of UCM1341 in counteracting inflammation-mediated neurodegeneration, FAAH activity was evaluated after drug exposure to a concentration of 10 μM. FAAH remained completely inhibited at all time-points (24-72 hours, Figure 5A). The levels of FAAH substrates AEA, OEA and PEA were also measured in the same conditions. While treatment with 10 μg/ml LPS + 100 ng/ml IFN-γ did not alter the concentrations of the three N-acylethanolamines, UCM1341 produced a significant increase of AEA and OEA concentrations at all time points, in line with the persistent inhibition of FAAH activity (Figure 5B-C). On the other hand, PEA levels were not affected by UCM1341 and remained at concentrations comparable to those of untreated samples (Figure 5D). We next evaluated the changes in GSH and GSSG levels, as markers of the cell oxidative stress. 10 DIV slices exposed to LPS +IFN-γ showed a trend to reduction of GSH availability at all time points. Treatment with UCM1341 did not affect GSH levels, nor the GSH/GSSG ratio (Figure 5E-F).

UCM1341 prevented TNFα release, upregulated the expression of the anti-inflammatory marker CD206, and increased AMPK phosphorylation in hippocampal explants

To address the effects of drug treatment on inflammatory response we analysed the expression of pro-inflammatory cytokines as well as markers of anti-inflammatory pathways. Quantitative ELISA analysis showed that LPS+IFN-γ exposure for 24-72 hours progressively increased the release of pro-inflammatory IL-6 and anti-inflammatory IL-10 cytokines (Figure 6A-B). Interestingly, UCM1341 prevented the release of TNFα in the medium and tissue lysates after 72 hours (Figure 6C), while the levels of IL-6, and IL-10 were not affected (Figure 6A-B). Immunoblotting and confocal double immunofluorescence staining revealed that the protein levels of the mannose receptor CD206, an M2

macrophage marker, and the number of CD206$^+$ stained cells were significant higher in drug-exposed slices after 72 hours of LPS+IFN-γ exposure (Figure 6D-E), thus suggesting an effect of UCM1341 on microglia polarization.

Recently, the activation of the monophosphate-activated protein kinase (AMPK), a serine/threonine kinase regulating cellular energy homeostasis, emerged as a negative regulator of inflammation and a "metabolic master switch" of macrophage polarization (Trefts and Shaw, 2021). Based on these μM UCM1341 treatment observations we hypothesized that the inflammation suppressive effects of UCM1341 might involve AMPK activation. Immunoblot showed that 10 for 72 hours significantly increased phospho-AMPK levels if compared to LPS+IFN-γ treated explants (Figure 6F).

UCM1341 stimulated the formation of lipid laden-foamy microglia/macrophages, and cholesterol homeostasis during LPS+IFN-γ-induced neuroinflammation

UCM1341 significantly prevented the loss of microglia and astrocytes 96 hours after the inflammatory injury, as revealed by the significantly higher number of Iba1$^+$ cells and GFAP$^+$ area measured in the CA1 region if compared to untreated cultures (Figure 7). Morphological assessment of Iba1$^+$ cells showed that dystrophic microglia dominate in the CA1 subfield of LPS+IFN-γ-exposed explants after 96 hours, while the foamy microglia/macrophages phenotype was clearly prevalent in slices treated with 10 μM UCM1341 during the inflammatory insult (Figure 7D-E)

Recent evidence indicated that the expression of nuclear and plasma membrane receptors coupling lipid metabolism to efficient cholesterol recycling in foamy macrophages is important for an efficient phagocytosis and cholesterol efflux in response to demyelination and, consequently, for CNS inflammation resolution and remyelination (Gouna et al., 2021). Thus, we explored the effect of UCM1341 treatment on lipid-laden macrophage formation and the expression of protein regulating cholesterol metabolism and efflux. UCM1341 treatment upregulated the protein levels of TREM2 (Figure 8A), a lipid sensor receptor that licences phagocytosis (Gouna et al., 2021), the cholesterol-sensing nuclear receptor LXR, and the cholesterol efflux ABCA1 transporter (Figure 8B), if compared to untreated and LPS + IFN-γ treated slices. Confocal analysis showed that Iba1$^+$ microglia/macrophages in the CA1 regions of UCM1341-treated explants abundantly coexpressed not only the lipid droplet marker Plin2 (Figure 8C) but also the cholesterol transporter ABCA1, if compared to LPS+IFN-γ treated slices (Figure 8D).

The PPARα, TRPV1, and MT/MT2 receptors significantly contributed to the neuroprotective effect of UCM1341

To investigate the role of EC and melatonin receptors on UCM1341 protective effects against LPS + IFN-γ-induced neuroinflammation in hippocampal explants, we examined the possible interference of specific antagonists of CB1, CB2, TRPV1, PPARα, and melatonin receptors. Antagonists were used at concentrations that displayed no effect when used alone. As shown in Figure 9A-B, quantitative densitometric analysis of PI uptake revealed that the neuroprotective effect of 10 μM UCM1341 in the CA1 region was significantly prevented by the PPARα (10 μM GM6471) TRPV1 (30 nM SB366791), and melatonin receptor (0.1 μM luzindole) antagonists. Conversely, both the CB1 and CB2 antagonists, i.e 0.1 μM AM251 and 0.1 μM AM630, failed to antagonize UCM1341-induced neuroprotection in LPS + IFN-γ-treated cultures. Finally, to investigate the possible cross-talk of the EC and melatonergic systems, we explored the expression of PPARα protein levels at an early time after the inflammatory insult, in the absence or in the presence of UCM1341 or reference compounds. As shown in Figure 9C, the explant exposure to LPS + IFN-γ + 10 μM UCM1341, or + 10 μM URB597 + 10 μM MEL, for 8 hours, significantly increased the expression of PPARα levels if compared to untreated and LPS + IFN-γ-treated slices. These findings reveal that a cross-talk between the EC and melatonergic pathways via the early activation of PPARα may contribute to the beneficial effect of the bivalent ligand.

Discussion and Conclusions

The present study shows that the newly synthesized compound UCM1341, a bivalent ligand endowed with FAAH inhibitory activity and melatonin receptor agonism, exerts a greater neuroprotection against neuroinflammation-induced degeneration in hippocampal explants if compared to the reference compounds, URB597 or melatonin, and encourages inflammation resolution contributing to the formation of lipid-laden macrophages and the expression of proteins controlling cholesterol metabolism and efflux. The activation of PPARα, TRPV1, and melatonin receptors and a cross-talk between the EC and melatonergic systems contribute to the beneficial effects of UCM1341 during the neuroinflammatory insult. We showed that the neurodegeneration occurring in the CA1 hippocampal region after explants exposure to LPS+IFN-γ, a model of inflammatory degeneration, can be monitored by PI uptake. This model of damage recapitulates the main hallmarks of inflammatory demyelinating CNS diseases, including glia activation, axonal demyelination, and neuronal loss (Boscia et al., 2020; 2021), and can be used to study the effects of pharmacological agents against the neuroinflammatory damage.

Dysregulation of ECs levels and melatonin release and alteration of melatonin receptor expression take place in many chronic CNS inflammatory conditions and contribute to cell dysfunction and disease progression (Chiurchiu' et al., 2018; Reiter et al., 2013). We showed that FAAH levels early increased in hippocampal CA1 pyramidal neurons and astrocytes after the neuroinflammatory insult, and also emerged in microglia at later time points. In line, FAAH mRNA and protein levels increased in astrocytes at asymptomatic and acute experimental autoimmune encephalomyelitis (EAE) stage and in glial cells surrounding Aβ plaques in AD and Down syndrome brain tissue (Benito et al., 2003; Benito et al., 2007; Nu´n˜ez et al., 2008; Moreno-García et al., 2020). Conversely, melatonin deficiency and a decline of MT receptor levels have been described in PD, AD, and ALS brains (Savaskan et al., 2005; Adi et al., 2010; Zhang et al., 2013). Interestingly, in AD brain, MT1 density increased in hippocampal pyramidal neurons, while MT2 levels decreased (Savaskan et al., 2002). Consistently, our biochemical studies showed that MT2 receptors, but not MT1, decreased after a transient upregulation following LPS+IFN-γ exposure. Whether the imbalance between MT1 and MT2 levels may reflect a compensatory effect, and to what extent it is associated with signalling differences in neurons and glia under neuroinflammatory conditions remains to be investigated.

Our studies showed that UCM1341 exerted a greater neuroprotection against the neuroinflammatory damage than against the NMDA insult, and attenuated axonal demyelination and gabaergic loss.

In support of the higher beneficial role of FAAH inhibition on the inflammatory component of damage, previous studies showed that URB597 significantly attenuated excitotoxic neurodegeneration when only a mild insult was applied (Mikheeva et al., 2017). This latter

observation may support our results showing the predominant contribution of the melatonergic component to the protective action of UCM1341 under excitotoxic conditions.

The protective effects of ECs and melatonin have been largely documented in a plethora of pathological states, particularly in disorders in which the neuroinflammatory component plays a central role, such as MS and AD. FAAH inhibition or melatonin treatment, via pharmacological modulation or genetic ablation, attenuated Aβ accumulation, neuroinflammation, and cognitive decline in experimental models of AD, and ameliorated EAE severity and remission in mice (Rossi et al, 2011; Piro et al., 2012; Wen et al., 2016; Corpas et al., 2018; Ghareghani et al., 2019*).*

A relevant result of our study is the finding that the reference compounds, URB597 and melatonin, when used in combination (both at 10 μM), exerted a synergistic neuroprotective action against the neuroinflammatory damage, an effect that was comparable to that of 10 μM UCM1341. This suggest not only that both lipid ethanolamine signalling and melatonin receptors activation are required for UCM1341 actions but also that an interplay between the EC and melatonergic systems might contribute to its beneficial effects. In support, we found that the blockade of PPARα, TRPV1, and melatonin receptors, but not of CB1 and CB2 receptors, prevented the neuroprotective actions of UCM1341. Remarkably, we showed that UCM1341 fully inhibited FAAH activity and significantly rose the hippocampal levels of AEA and OEA, the endogenous ligands of TRPV1 and PPARα, respectively (Muller et al., 2019). The reason why we were unable to detect an increase in PEA levels is unknown. Previous studies have suggested a region-specific alteration in brain N-acylethanolamine levels following inhibition of ECs degrading enzymes, or it can be possibly due to a time- and-spatial restricted distribution (Bortolato et al., 2007; Henry et al., 2014). On the other hand, PEA hydrolysis is sustained not only by FAAH, but also by the enzyme N-acylethanolamine acid amidase (NAAA), whose inhibition in activated inflammatory cells leads to a normalization of PEA levels (Solorzano et al., 2009; Piomelli et al., 2020).

The protective activity of UCM1341 was counteracted by luzindole, and MT1/MT2 melatonin receptor antagonist, sustaining a receptor-dependent mechanism for the melatonergic component. Melatonin and related indole-derivatives are widely reported as direct antioxidant agents conferring cellular protection from radical species and prooxidant mediators (Reiter et al., 2013). Nevertheless, in hippocampal slices we observed no effect of UCM1341 on GSH levels and on the balance between the reduced and oxidized species. Recent experimental evidence supports the involvement of melatonin membrane receptors, and in particular of the MT1 subtype, in mediating its neuroprotective activity. Indeed, melatonin receptor activation modulates the activity of transcription factors which in turn decrease the expression of proinflammatory mediators, induce antioxidant genes and promote a shift of microglia toward an M2 phenotype (Zhou et al., 2021; Liu etl., 2022). A further support for

the receptor-mediated neuroprotective activity of melatonergic agents comes from the improvement of LPS-induced neuroinflammation exerted by the receptor agonist ramelteon, devoid of the indole nucleus, and counteracted by luzindole (Gu et al., 2021).

In support of the synergistic action between the EC and melatonergic systems, we showed that both UCM1341 and combined melatonin + URB597 explant exposure, increased the expression of PPARα levels during the neuroinflammatory insult. Previous studies have suggested that the upregulation and activation of PPARα receptors contributed not only to the neuroprotective and anti-inflammatory actions of its endogenous ligand OEA (Sun et al., 2007;), but also of melatonin. For instance, Paterniti et al. (2017) showed that the beneficial effects of melatonin on spinal cord tissue injury and pro-inflammatory cytokine release were significantly reduced in PPARα knock-out mice.

The central role of TRPV1 channels in glia to neuron communication during neuroinflammation is largely documented (Marrone et al., 2017). Although the consequence of its modulation under neuroinflammatory conditions remains controversial (Boscia et al., 2021), our data support the anti-inflammatory effects of TRPV1 activation. Moreover, previous studies showed that PPARα and TRPV1 receptors functionally and biochemically interacted (Ambrosino et al., 2014), thus suggesting that the cross-talk between these two receptors may also contribute to UCM1341 effects.

PPARα is a ligand-dependent transcription factor that mediates the transrepression of the main inflammatory transcription factors and acts as a master regulator of lipid metabolism and cholesterol homeostasis (Chinetti et al., 2001). Previous studies showed that ECs and some N-acylethanolamides, particularly OEA, and melatonin act as immunomodulators controlling innate immune activation and cytokine release (Chiurchiù et al., 2018). In line, our findings suggest that UCM1341 sustains a pro-resolving macrophage behavior during neuroinflammation, as reported for both URB597 and melatonin (Mecha et al., 2015; Tanaka et al., 2019; Grieco et al., 2021; Hardeland et al., 2021). Indeed, in response to the pro-inflammatory insult, the bivalent ligand prevented the release of TNFα, a cytokine sustaining the pro-inflammatory activation of microglia, and upregulated the mannose CD206 receptor, an anti-inflammatory macrophage M2 marker. Consistent with the UCM1341-induced synergistic activation of protective ECs and melatonergic signalling pathways, we showed that during neuroinflammation UCM1341 upregulated the levels of phosphorylated AMP kinase, an important cellular energy sensor that represses pro-inflammatory responses, and favors microglia M2 polarization (Trefts and Shaw, 2021).

It is now clear that in the absence of proper cholesterol metabolism der conditions of myelin phagocytic activity, macrophages exhibit dysregulated inflammatory responses, phagocyte dysfunction and altered immune functions and tissue regeneration (Berghoff et al., 2021). Our findings, by showing that UCM1341 polarized macrophages to a lipid-laden Plin2^{+} foamy phenotype,

upregulated the phagocytic receptor TREM2, the lipid-sensing nuclear receptors LXR, and the cholesterol efflux transporters ABCA1, suggest a role of the bivalent ligand in sustaining a restorative response against a neuroinflammatory demyelinating insult through the modulation of cholesterol metabolism. In support, the upregulation of ABCA1 contribute to the protective and anti-atherosclerotic properties of both OEA and melatonin (Chinetti et al., 2001; Kim et al., 2021).

Collectively, our findings reveal that UCM134, by inhibiting FAAH enzyme and stimulating PPARα, TRPV1, and melatonin receptors modulates the expression of receptors and intracellular signaling pathways governing CNS protective and inflammation resolution responses. Future work is needed to determine the impact of joint targeting EC and melatonergic systems in models of neurodegenerative disease-associated inflammatory states.

References

Franklin, R.J.M., Ffrench-Constant C. (2017) Regenerating CNS myelin - from mechanisms to experimental medicines. *Nature Review Neuroscience,* 18(12), 753-769. doi: 10.1038/nrn.2017.136.

Boscia F., Elkjaer M.L., Illes Z., Kukley M. (2021) Altered Expression of Ion Channels in White Matter Lesions of Progressive Multiple Sclerosis: What Do We Know About Their Function? Front *Cell Neuroscience,* 15:685703. doi: 10.3389/fncel.2021.685703.

Chiurchiù V., van der Stelt M., Centonze D., Maccarrone M. (2018) The endocannabinoid system and its therapeutic exploitation in multiple sclerosis: Clues for other neuroinflammatory diseases. *Progress in Neurobiolology,* 160, 82–100. doi: 10.1016/j.pneurobio.10.007.

Reiter R.J., Tan D.X., Rosales-Corral S., Manchester L.C. (2013) The universal nature, unequal distribution and antioxidant functions of melatonin and its derivatives. *Mini-Review in Medicinal Chemistry,* 13(3), 373-84. doi: 10.2174/1389557511313030006.

Piomelli D. (2003) The molecular logic of endocannabinoid signalling. *Nature Review Neuroscience,* 4(11), 873-84. doi: 10.1038/nrn1247.

Petrosino S., Di Marzo V. (2010) FAAH and MAGL inhibitors: therapeutic opportunities from regulating endocannabinoid levels. *Current Opinion Investigional Drugs*, 11(1), 51-62. PMID: 20047159.

van Egmond N., Straub V.M., van der Stelt M. (2021) Targeting Endocannabinoid Signaling: FAAH and MAG Lipase Inhibitors. *Annual Review Pharmacology Toxicology*, 61, 441-463. doi: 10.1146/annurev-pharmtox-030220-112741.

Kopustinskiene D.M., Bernatoniene J. (2021) Molecular Mechanisms of Melatonin-Mediated Cell Protection and Signaling in Health and Disease. *Pharmaceutics,* 13(2), 129. doi: 10.3390/pharmaceutics13020129.

Spadoni G., Bedini A., Furiassi L., Mari M., Mor M., Scalvini L., Lodola A., Ghidini A., Lucini V., Dugnani S., Scaglione F., Piomelli D., Jung K.M., Supuran C.T., Lucarini L., Durante M., Sgambellone S., Masini E., Rivara S. (2018) Identification of Bivalent Ligands with Melatonin Receptor Agonist and Fatty Acid Amide Hydrolase (FAAH) Inhibitory Activity That Exhibit Ocular Hypotensive Effect in the Rabbit. *Journal of Medicinal Chemistry*, 61(17), 7902-7916. doi: 10.1021/acs.jmedchem.8b00893.

Boscia F., Annunziato L., Taglialatela M. (2006) Retigabine and flupirtine exert neuroprotective actions in organotypic hippocampal cultures. *Neuropharmacology,* 51(2), 283-294. doi: 10.1016/j.neuropharm.

Boscia F., Ferraguti F., Moroni F., Annunziato L., Pellegrini-Giampietro D.E. (2008) mGlu1alpha receptors are co-expressed with CB1 receptors in a subset of interneurons in the CA1 region of organotypic hippocampal slice cultures and adult rat brain. *Neuropharmacology*, 55(4), 428-439. doi: 10.1016/j.neuropharm.2008.04.024.

Papageorgiou I.E., Lewen A., Galow L.V., Cesetti T., Scheffel J., Regen T., Hanisch U.K., Kann O. (2016) TLR4-activated microglia require IFN-γ to induce severe neuronal dysfunction and death in situ. *Proc Natl Acad Sci U S A*, 113(1) 212-7. doi: 10.1073/pnas.1513853113

Landucci E., Mazzantini C., Lana D., Davolio P.L., Giovannini M.G., Pellegrini-Giampietro D.E. (2021) Neuroprotective Effects of Cannabidiol but Not Δ9-Tetrahydrocannabinol in Rat Hippocampal Slices Exposed to Oxygen-Glucose Deprivation: Studies with Cannabis Extracts and Selected Cannabinoids. *International Journal Molecular Sciences*, 22(18), 9773. doi: 10.3390/ijms22189773.

Boscia F., Passaro C., Gigantino V., Perdonà S., Franco R., Portella G., Chieffi S., Chieffi P. (2015) High levels of GPR30 protein in human testicular carcinoma in situ and seminomas correlate with low levels of estrogen receptor-beta and indicate a switch in estrogen responsiveness. *Journal Cell Physiology, 230*(6), 1290-1297. doi: 10.1002/jcp.24864.

Cammarota M., de Rosa V., Pannaccione A., Secondo A., Tedeschi V., Piccialli I., Fiorino F., Severino B., Annunziato L., Boscia F. (2021) Rebound effects of NCX3 pharmacological inhibition: A novel strategy to accelerate myelin formation in oligodendrocytes. *Biomedicine and Pharmacotherapy*, 143, 112111. doi: 10.1016/j.biopha.2021.112111.

Boscia F., Esposito C.L., Casamassa A., de Franciscis V., Annunziato L., Cerchia L. (2013) The isolectin IB4 binds RET receptor tyrosine kinase in microglia. *Journal of Neurochemistry,* 126(4), 428-436. doi: 10.1111/jnc.12209. Epub 2013 Mar 17.

de Rosa V., Secondo A., Pannaccione A., Ciccone R., Formisano L., Guida N., Crispino R., Fico A., Polishchuk R., D'Aniello A., Annunziato L., Boscia F. (2019) D-Aspartate treatment attenuates myelin damage and stimulates myelin repair. *EMBO Molecular Medicine,* 11(1), e9278. doi: 10.15252/emmm.201809278.

Casamassa A., La Rocca C., Sokolow S., Herchuelz A., Matarese G., Annunziato L., Boscia F. (2016) Ncx3 gene ablation impairs oligodendrocyte precursor response and increases susceptibility to experimental autoimmune encephalomyelitis. *Glia,* 64(7), 1124-1137. doi: 10.1002/glia.22985.

Boscia F., Esposito C.L., Di Crisci A., de Franciscis V., Annunziato L., Cerchia L. (2009) GDNF selectively induces microglial activation and neuronal survival in CA1/CA3 hippocampal regions exposed to NMDA insult through Ret/ERK signalling. *PLoS One,* 4(8), e6486. doi: 10.1371/journal.pone.0006486.

Vincenzi F., Ravani A., Pasquini S., Merighi S., Gessi S., Setti S., Cadossi R., Borea PA., Varani K. (2017). Pulsed Electromagnetic Field Exposure Reduces Hypoxia and Inflammation Damage in Neuron-Like and Microglial Cells. *J Cell Physiol,* 232(5), 1200-1208. doi: 10.1002/jcp.25606.

Carnevali L., Statello R., Vacondio F., Ferlenghi F., Spadoni G., Rivara S., Mor M., Sgoifo A. (2020) Antidepressant-like effects of pharmacological inhibition of FAAH activity in socially isolated female rats. *European Neuropsychopharmacology,* 32, 77-87. doi: 10.1016/j.euroneuro.2019.12.119.

Clapper J.R., Vacondio F., King A.R., Duranti A., Tontini A., Silva C., Sanchini S., Tarzia G., Mor M., Piomelli D. (2009) A second generation of carbamate-based fatty acid amide hydrolase inhibitors with improved activity in vivo. *Chem Med Chem,* 4(9), 1505-1513. doi: 10.1002/cmdc.200900210.

Curtis M.J., Alexander S., Cirino G., Docherty J.R., George C.H., Giembycz M.A., Hoyer D., Insel P.A., Izzo A.A., Ji Y., MacEwan D.J., Sobey C.G., Stanford S.C., Teixeira M. M., Wonnacott S., & Ahluwalia A. (2018) Experimental design and analysis and their reporting II: Updated and simplified guidance for authors and peer reviewers. *British Journal of Pharmacology,*175(7), 987–993.https://doi.org/10.1111/bph.14153

Gulyas A.I., Cravatt B.F., Bracey M.H., Dinh T.P., Piomelli D., Boscia F., Freund T.F. (2004) Segregation of two endocannabinoid-hydrolyzing enzymes into pre- and postsynaptic compartments in the rat hippocampus, cerebellum and amygdala. *European Journal of Neuroscience,* 20(2), 441-458. doi: 10.1111/j.1460-9568.2004.03428.x.

Trefts E., Shaw R.J. (2021): restoring metabolic homeostasis over space and time. *Molecular Cell,* 81(18), 3677-3690. doi: 10.1016/j.molcel.2021.08.015.

Gouna G., Klose C., Bosch-Queralt M., Liu Lu., Gokce Ozgun., Schifferer Martina., Cantuti-Castelvetri L., Simons M., (2021) TREM2-dependent lipid droplet biogenesis in phagocytes is required for remyelination *Journal of Experiment Medicine*, 218 (10), e20210227. doi.org/10.1084/jem.20210227

Boscia F., de Rosa V., Cammarota M., Secondo A., Pannaccione A., Annunziato L. (2020) The Na^+/Ca^{2+} exchangers in demyelinating diseases. *Cell Calcium,* 85:102130. doi: 10.1016/j.ceca.2019.102130.

Benito C., Núñez E., Tolón R.M., Carrier E.J., Rábano A., Hillard C.J., Romero J. (2003) Cannabinoid CB2 receptors and fatty acid amide hydrolase are selectively overexpressed in neuritic plaque-associated glia in Alzheimer's disease brains. *Journal of Neuroscience,* 23(35), 11136-41. doi: 10.1523/jneurosci.23-35-11136.2003.

Benito C., Romero J.P., Tolón R.M, Clemente D., Docagne F., Cecilia J., Hillard C., Guaza and Julián R. (2007) Cannabinoid CB1 and CB2 receptors and fatty acid amide hydrolase are specific markers of plaque cell subtypes in human multiple sclerosis. *Journal of Neuroscience*, 27, 2396–2402 doi: 10.1523/jneurosci.4814-06.2007.

Núñez E., Benito C., Tolón R.M., Hillard C.J., Griffin W.S., Romero J, (2008) Glial expression of cannabinoid CB (2) receptors and fatty acid amide hydrolase are beta amyloid-linked events in Down's syndrome. *Neuroscience*, 151(1), 104-10. doi: 10.1016/j.neuroscience.

Moreno-García Á., Bernal-Chico A., Colomer T., Rodríguez-Antigüedad A., Matute C., Mato S, (2020) Gene Expression Analysis of Astrocyte and Microglia Endocannabinoid Signaling during Autoimmune Demyelination. *Biomolecules,* 10(9), 1228. doi: 10.3390/biom10091228.

Savaskan E., Ayoub M.A., Ravid R., Angeloni D., Fraschini F., Meier F., Eckert A., Müller-Spahn F, Jockers R. (2005) Reduced hippocampal MT2 melatonin receptor expression in Alzheimer's disease. *Journal of Pineal Research,* 38(1), 10-6. doi: 10.1111/j.1600-079X.2004.00169.x.

Adi N., Mash D.C., Ali Y., Singer C., Shehadeh L., Papapetropoulos S. (2010) Melatonin MT1 and MT2 receptor expression in Parkinson's disease *Medical Science Monitor*, 16(2), BR61-7.

Zhang Y., Cook A., Kim J., Baranov S.V., Jiang J., Smith K., Cormier K., Bennett E., Browser R.P., Day A.L., Carlisle D.L., Ferrante R.J., Wang X., Friedlander R.M. (2013) Melatonin inhibits the caspase-1/cytochrome c/caspase-3 cell death pathway, inhibits MT1 receptor loss and delays disease progression in a mouse model of amyotrophic lateral sclerosis. *Neurobiology Disease,* 55, 26-35. doi: 10.1016/j.nbd.2013.03.008.

Savaskan E., Olivieri G., Meier F., Brydon L., Jockers R., Ravid R., Wirz-Justice A., Müller-Spahn F. (2002) Increased melatonin 1a-receptor immunoreactivity in the hippocampus of Alzheimer's disease patients. *Journal of Pineal Research,* 32(1), 59-62. doi: 10.1034/j.1600-079x.2002.00841.x.

Mikheeva I.B., Shubina L., Matveeva N., Pavlik L.L., Kitchigina V.F. (2017) Fatty acid amide hydrolase inhibitor URB597 may protect against kainic acid-induced damage to hippocampal neurons: Dependence on the degree of injury. *Epilepsy Research,* 137, 84-94. doi: 10.1016/j.eplepsyres.2017.09.017.

Rossi S., Furlan R., De Chiara V., Muzio L., Musella A., Motta C., Studer V., Cavasinni F., Bernardi G., Martino G., Cravatt B.F., Lutz B., Maccarrone M., Centonze D. (2011) Cannabinoid CB1 receptors regulate neuronal TNF-α effects in experimental autoimmune encephalomyelitis. *Brain Behavior and Immunity,* 25(6), 1242-1248. doi: 10.1016/j.bbi.2011.03.017.

Piro J.R., Benjamin D.I., Duerr J.M., Pi Y., Gonzales C., Wood K.M., Schwartz J.W., Nomura D.K., Samad T.A. (2012) A dysregulated endocannabinoid-eicosanoid network supports pathogenesis in a mouse model of Alzheimer's disease. *Cell Reports,* 1, 61723. doi: 10.1016/j.celrep.2012.05.001

Wen J., Ariyannur P.S., Ribeiro R., Tanaka M., Moffett J.R., Kirmani B.F., Namboodiri A.M., Zhang Y. (2016) Efficacy of N-Acetylserotonin and Melatonin in the EAE Model of Multiple Sclerosis. *Journal Neuroimmune Pharmacology*, 11(4), 763-773. doi: 10.1007/s11481-016-9702-9.

Corpas R., Griñán-Ferré C., Palomera-Ávalos V., Porquet D., García de Frutos P., Franciscato Cozzolino S.M., Rodríguez-Farré E., Pallàs M., Sanfeliu C., Cardoso B.R. (2018) Melatonin induces mechanisms of brain resilience against neurodegeneration. *Journal Pineal Research*, 65(4), e12515. doi: 10.1111/jpi.12515.

Ghareghani M., Scavo L., Jand Y., Farhadi N., Sadeghi H., Ghanbari A., Mondello S., Arnoult D., Gharaghani S., Zibara K. (2019) Melatonin Therapy Modulates Cerebral Metabolism and Enhances Remyelination by Increasing PDK4 in a Mouse Model of Multiple Sclerosis. *Frontiers Pharmacology,* 10, 147. doi: 10.3389/fphar.2019.00147.

Muller C., Morales P., Reggio P.H. (2019) Cannabinoid Ligands Targeting TRP Channels. *Frontiers Molecular Neuroscience*, 11, 487. doi: 10.3389/fnmol.2018.00487.

Bortolato M., Mangieri R.A., Fu, J., Kim J.H., Arguello O., Duranti A., Tontini, A., Mor, M., Tarzia, G., Piomelli, D. (2007) Antidepressant-like activity of the fatty acid amide hydrolase

inhibitor URB597 in a rat model of chronic mild stress. *Biology Psychiatry,* 62, 1103–1110. doi: 10.1016/j.biopsych.2006.12.001.

Henry R.J., Kerr D.M., Finn D.P., Roche M. (2014) FAAH-mediated modulation of TLR3-induced neuroinflammation in the rat hippocampus. *Journal Neuroimmunology,* 276 (1-2), 126-134. doi: 10.1016/j.jneuroim.2014.09.002.

Solorzano C., Zhub C., Battista N., Astarita G., Lodolae A., Rivara S., Mor M., Russo R., Maccarrone M., Antonietti F., Duranti A., Tontini A., Cuzzocrea S., Tarzia G., Piomelli D. (2009) Selective N-acylethanolamine-hydrolyzing acid amidase inhibition reveals a key role for endogenous palmitoylethanolamide in inflammation. *Proc Natl Acad Sci U S A,* 106(49):20966-71. doi: 10.1073/pnas.0907417106.

Piomelli D, Scalvini L., Fotio Y., Lodola A., Spadoni G., Tarzia G., Mor M. (2020) N-Acylethanolamine Acid Amidase (NAAA): Structure, Function, and Inhibition. *Journal of Medicinal Chemistry,* 63(14), 7475-7490. doi: 10.1021/acs.jmedchem.0c00191

Zhou Q., Lin L., Wang H., Jiang S., Huang P., Lin Q., Chen X., Deng Y. (2021) Melatonin Reduces Neuroinflammation and Improves Axonal Hypomyelination by Modulating M1/M2 Microglia Polarization via JAK2-STAT3-Telomerase Pathway in Postnatal Rats Exposed to Lipopolysaccharide. *Molecular Neurobiology*, 58(12), 6552-6576. doi: 10.1007/s12035-021-02568-7.

Liu X., Yao S., Bi J., Zheng D., Wang P. (2022) Protective effects and regulatory mechanisms of melatonin in a neonatal mouse model of LPS-induced inflammation. *Neuroscience Letters, 16*, 772:136483. doi: 10.1016/j.neulet.2022.136483.

Gu C., Wang F., Zhang Y.T., Wei S.Z., Liu J.Y., Sun H.Y., Wang G.H., Liu C.F. (2021) Microglial MT1 activation inhibits LPS-induced neuroinflammation via regulation of metabolic reprogramming. *Aging Cell,* 20(6), e13375. doi: 10.1111/acel.13375.

Sun Y., Alexander S.P., Garle M.J., Gibson C.L., Hewitt K., Murphy S.P., Kendall D.A., Bennett A.J. (2007) Cannabinoid activation of PPAR alpha; a novel neuroprotective mechanism. *British Journal Pharmacology,* 152(5), 734-43. doi: 10.1038/sj.bjp.0707478.

Paterniti I., Campolo M., Cordaro M., Impellizzeri D., Siracusa R., Crupi R., Esposito E., Cuzzocrea S. (2017) PPAR-α Modulates the Anti-Inflammatory Effect of Melatonin in the Secondary Events of Spinal Cord Injury, *Molecular Neurobiology,* 54(8), 5973-5987. doi: 10.1007/s12035-016-0131-9.

Marrone M.C., Morabito A., Giustizieri M., Chiurchiù V., Leuti A., Mattioli M., Marinelli S., Riganti L., Lombardi M., Murana E., Totaro A., Piomelli D., Ragozzino D., Oddi S., Maccarrone M., Verderio C., Marinelli S. (2017) TRPV1 channels are critical brain inflammation detectors and neuropathic pain biomarkers in mice. *Nature Communication,* 10, 8:15292. doi: 10.1038/ncomms15292.

Ambrosino P., Soldovieri M.V., De Maria M., Russo C., Taglialatela M. (2014) Functional and biochemical interaction between PPARα receptors and TRPV1 channels: Potential role in PPARα

agonists-mediated analgesia. *Pharmacology Research,* 87, 113-22. doi: 10.1016/j.phrs.2014.06.015.

Chinetti G., Lestavel S., Bocher V., Remaley A.T., Neve B., Torra I.P., Teissier E., Minnich A., Jaye M., Duverger N., Brewer H.B., Fruchart J.C., Clavey V., Staels B. (2001) PPAR-alpha and PPAR-gamma activators induce cholesterol removal from human macrophage foam cells through stimulation of the ABCA1 pathway. *Nature Medicine,* 7(1), 53-8. doi: 10.1038/83348.

Mecha M., Feliú A., Carrillo-Salinas F.J, Rueda-Zubiaurre A., Ortega-Gutiérrez S., García de Sola R., Guaza C. (2015) Endocannabinoids drive the acquisition of an alternative phenotype in microglia *Brain Behavior Immunology,* 49, 233-245. doi: 10.1016/j.bbi.2015.06.002.

Tanaka M., Yagyu K., Sackett S., Zhang Y. (2019) Anti-Inflammatory Effects by Pharmacological Inhibition or Knockdown of Fatty Acid Amide Hydrolase in BV2 Microglial *Cells Cells,* 8, 491. doi: 10.3390/cells8050491.

Grieco M., De Caris M.G., Maggi E., Armeli F., Coccurello R., Bisogno T., D'Erme M., Maccarrone M., Mancini P., Businaro R. (2021) Fatty Acid Amide Hydrolase (FAAH) Inhibition Modulates Amyloid-Beta-Induced Microglia Polarization, *International Journal of Molecular Science,* 22, 771. doi: 10.3390/ijms22147711.

Hardeland R. (2021) Melatonin and Microglia. *International Journal Molecular Science*, 22(15), 8296. doi: 10.3390/ijms22158296.

Berghoff S.A., Spieth L., Sun T., Hosang L., Schlaphoff L., Depp C., Düking T., Winchenbach J., Neuber J., Ewers D., Scholz P., van der Meer F., Cantuti-Castelvetri L., Sasmita A.O., Meschkat M., Ruhwedel T., Möbius W., Sankowski R., Prinz M., Huitinga I., Sereda M.W., Odoardi F., Ischebeck T., Simons M., Stadelmann-Nessler C., Edgar J.M., Nave K.A., Saher G. (2021) Microglia facilitate repair of demyelinated lesions via post-squalene sterol synthesis. *Nature Neuroscience,* 24(1), 47-60. doi: 10.1038/s41593-020-00757-6.

Kim J.S., Jung Y.H., Lee H.J., Chae C.W., Choi G.E., Lim J.R., Kim S.Y., Lee J.E., Han H.J. (2021) Melatonin activates ABCA1 via the BiP/NRF1 pathway to suppress high-cholesterol-induced apoptosis of mesenchymal stem cells. *Stem Cell Res Ther*, 12(1):114. doi: 10.1186/s13287-021-02181-4.

Legend to figures

Figure 1. Dose-dependent effects of UCM1341 against NMDA-induced neurodegeneration in hippocampal explants. **A-B,** PI fluorescence staining patterns (a-d) and densitometric quantification of PI uptake in hippocampal CA1 and CA3 subfields (e-f) measured 48 hours following 10 μM NMDA (A) or 30 μM NMDA (B) exposure in the absence or in the presence of 0.1-10 μM UCM1341, respectively. Scale bars in a-d: 500 μm. **C,** PI fluorescence staining patterns (a-d) and densitometric quantification of PI uptake in hippocampal CA1 and CA3 subfields (e-f) measured 48 hours following 10 μM NMDA exposure in the absence or in the presence of 10 μM melatonin, 10 μM URB597, 10 μM melatonin + 10 μM URB597. Scale bars in a-d: 500 μm. Data are normalized as percentage of control. The values represent the mean±S.E.M (n = 5). One-way ANOVA with Bonferroni post hoc analysis. *$p < 0.05$ versus NMDA.

Figure 2. Time-dependent effects of LPS+IFN–γ exposure on PI uptake, and Iba1, MBP, FAAH and melatonin receptor protein levels in rat hippocampal explants. A-B, Representative images (a-b) and quantitative densitometric analysis (c) of PI fluorescence uptake recorded in the CA and DG subfields of 7 DIV slices (A) or 10 DIV slices (B) exposed to LPS + IFN-γ for 72 or 96 hours, respectively. Data are expressed as percentage of the maximal value of PI fluorescence observed in the CA1 subregion upon 72 or 96 hours of LPS + IFN-γ exposure, respectively. Each data point is the mean±S.E.M. (n=5). Scale bars in a-b: 500 μm. **C-E**, Western blot (C) and quantification of Iba1 (D) and melatonin MT1/MT2 receptor (E) protein levels in hippocampal slices under control conditions and after LPS + IFN–γ exposure for 24-72 hours. Data were normalized on the basis of β-actin and expressed as percentage of controls. The values represent the mean±S.E.M. (n = 5). One-way ANOVA with Bonferroni post hoc analysis. *$p < 0.05$ versus respective control. **F-H**, Western blot (F) and quantification of FAAH (G) and MBP (H) protein levels in hippocampal slices under control conditions and after LPS + IFN-γ exposure for 24-72 hours. Data were normalized on the basis of β-actin and expressed as percentage of controls. The values represent the mean±S.E.M. (n = 5). One-way ANOVA with Bonferroni post hoc analysis. *$p < 0.05$ versus respective control. **F,** Representative confocal double immunofluorescence images displaying the distribution of MBP (red) and NF200 (green) immunoreactivities and their colocalization (white) in untreated (a, c, e) and LPS + IFN–γ treated (b, d, f) slices for 72 hours. Scale bar in a-f: 200 μm.

Figure 3. Distribution of FAAH immunoreactivity in neurons, astrocytes and microglia of hippocampal explants during LPS+IFN-γ exposure. A-B, Representative confocal images displaying the colocalization of FAAH with MAP2 (A) or FAAH with GFAP (B) immunoreactivities in the CA1 hippocampal region, in the absence (a–d) or in the presence of LPS + IFN-γ (e–h) for 24 hours. **C-D**, Confocal images displaying colocalization of FAAH with CD11b (C) or FAAH with GFAP (D) immunoreactivities in the CA1 hippocampal region, in the absence (a–d) or in the presence of LPS+IFN-γ (e–h) for 48 hours. In A-D, panels d and h display the colocalized points (white). Arrows in e-h point to colocalizing cells. Scale bars: 50μm. **E-F**, Quantitative analysis of FAAH, MAP2, GFAP, and CD11b immunofluorescence intensities (E) and FAAH colocalization with MAP2, GFAP, or CD11b immunosignals (F) in the CA1 hippocampal region, in the absence or in the presence of LPS+IFN-γ for 24 hours. **G-H,** Quantitative analysis of FAAH, MAP2, GFAP, and CD11b immunofluorescence intensities (G) and FAAH colocalization with MAP2, GFAP, and CD11b immunosignals (H) in the absence or in the presence of LPS+IFN-γ for 48 hours. Data were obtained from 5 microscope fields per slice in each group and expressed as percentage of control. The values represent the mean±S.E.M. (n=5). Unpaired Student's t-test. *$p < 0.05$ versus respective control.

Figure 4. Protective effects of UCM1341 against neuroinflammation-induced degeneration

A, PI fluorescence staining patterns (a-d) and quantitative densitometric analysis of PI uptake (e) in the CA1 region following LPS+IFN-γ–exposure in the absence or in the presence of 0.1-10 μM UCM1341 for 96 hours. The values represent the mean±S.E.M. (n=5). One-way ANOVA with Bonferroni post hoc analysis. *$p < 0.05$ versus LPS+IFN-γ. **B,** PI fluorescence staining patterns (a-d) and quantitative densitometric analysis of PI uptake (e) in the CA1 region following LPS+IFN-γ–exposure in the absence or in the presence of 10 μM melatonin, 10 μM URB597, 10 μM melatonin + 10 μM URB597, and 10 μM UCM1341 for 96 hours. The values represent the mean±S.E.M. (n=5). One-way ANOVA with Bonferroni post hoc analysis. *$p < 0.05$ versus LPS+IFN-γ. Scale bars in a-d: 500 μm. **C,** (a-c), Representative maximum intensity projection of z-stack confocal images displaying NF200 (green) and MBP (red) immunoreactivities in the CA1 region of 10 DIV hippocampal slices under control conditions (a-d), and LPS+IFN-γ exposure, in the absence (e-h) or in the presence of 10 μM UCM1341 (i-l) for 96 hours. Panels d, h, and l display colocalized points (white). Scale bars in a-l: 50 μm. (m), Quantitative analysis of NF200 immunofluorescence intensity under control conditions and in the presence of LPS+IFN-γ, and LPS+IFN-γ + 10 μM UCM1341. The values represent the mean±S.E.M. (n=5). One-way ANOVA with Bonferroni post hoc analysis.

*$p < 0.05$ versus control. ^$p < 0.05$ versus LPS+IFN-γ. (n), Analysis of the myelination index in the pyramidal/oriens layers of the CA1 region in 10 DIV hippocampal slices under control conditions and following LPS + IFN-γ exposure in the absence or in the presence of UCM1341. The values represent the mean±S.E.M. (n=5). One-way ANOVA with Bonferroni post hoc analysis. *$p < 0.05$ versus control. **D**, Representative confocal images (a-c) and quantitative analysis of GABA-positive cells (d) in the pyramidal layer of the CA1 hippocampal region, under control conditions or following LPS + IFN-γ in the absence (b) or in the presence (c) of UCM1341 for 96 hours. Scale bars in a-c: 50 μm. The values represent the mean±S.E.M. (n=5). One-way ANOVA with Bonferroni post hoc analysis. *$p < 0.05$ versus control. ^$p < 0.05$ versus LPS+IFN-γ.

Figure 5. Effect of UCM1341 on FAAH activity, and glutathione levels in hippocampal cultures. Fatty acid amide hydrolase (FAAH) activity (panel A), anandamide (AEA, panel B), N-oleoylethanolamine (OEA, panel C), N-palmitoylethanolamine (PEA, panel D), reduced glutathione (GSH, panel E) levels and GSH/GSSG ratios in organotypic hippocampal slices under control conditions or after LPS+IFN-γ exposure in the absence or in the presence of 10 μM UCM1341 for 24-72 hours (Ctrl, light gray bars); LPS+IFN-γ (black bars); Ctrl+10 μM UCM1341 (white bars); LPS+IFN-γ+ 10 μM UCM1341 (green/gray bars). Results are expressed as mean value±S.E.M (n=5). One-way ANOVA with Bonferroni post hoc analysis. *$p<0.05$ if compared to corresponding control experiment.

Figure 6. Effect of UCM1341 on TNFα release, CD206 expression, and AMPK phosphorylation. A-B, Time-dependent production of IL-6 (A) and IL-10 (B) in the medium of explants cultures under control conditions or LPS+IFN-γ exposure in the absence or in the presence of 10 μM UCM1341 for 24-72 hours. Results are expressed as mean values ± S.E.M. (n=3). **C,** TNFα determination in the medium (left) and tissue lysates (right) of hippocampal cultures under control conditions, and LPS+IFN-γ exposure in the absence or in the presence of 10 μM UCM1341 for 72 hours. Results are expressed as mean values ± S.E.M. Experiments were performed in duplicate. **D,** Western blot and densitometric analysis of CD206 protein levels in hippocampal lysates under control conditions and after LPS+ IFN–γ exposure in the absence or in the presence of 10 μM UCM134 for 72 hours. Data were normalized on the basis of β-actin levels and expressed as percentage of control. The values represent the mean±S.E.M. (n = 5). One-way ANOVA with Bonferroni post hoc analysis. * $p < 0.05$ versus control. ^ $p < 0.05$ versus control and LPS+ IFN-γ. **E,** (a-i)**,** Representative confocal microscopic images showing CD206 and CD11b immunoreactivities in the CA1 hippocampal region

under control conditions, LPS + IFN-γ exposure, and LPS+IFNγ + 10 μM UCM1341. Scale bar: 20μm **E,** (j), Quantitative analysis of $CD206^+$ cells in slices under control conditions, and LPS+IFN-γ, LPS+IFN-γ + 10 μM UCM1341 exposure for 72 hours. Data are expressed as percentage of control. The values represent the mean±S.E.M. (n=5). One-way ANOVA with Bonferroni post hoc analysis. * $p < 0.05$ versus control. ^ $p < 0.05$ versus LPS+ IFN-γ. **F,** Western blot and densitometric analysis of pAMPK levels in hippocampal slices under control conditions and after LPS+IFN-γ exposure for 72 hours or in the presence of 10 μM UCM1341. Data were normalized on the basis of AMPK levels and expressed as percentage of control. The values represent the mean±S.E.M. (n = 5). One-way ANOVA with Bonferroni post hoc analysis. * $p < 0.05$ versus control and LPS+ IFN-γ .

Figure 7. Effect of UCM1341 on microglia and astrocyte immunoreactivities following LPS+IFN-γ exposure. A, Representative confocal microscopic images showing Iba1 (green) and GFAP (red) immunoreactivities in the CA1 hippocampal region of cultures under control conditions and after LPS+IFN-γ exposure in the absence or in the presence of 10 μM UCM1341 for 96 hours. Panels b-f show higher magnification images of squared areas in a-c. Arrows in d and f point to dystrophic or foamy microglia/macrophages, respectively. Scale bars in a, c, e: 200 μM; in b, d, f: 20 μm. **B-C**, Quantitative analysis of $Iba1^+$ cells (B) and $GFAP^+$ area (C) in control cultures, LPS+IFN-γ–treated cultures, in the absence or in the presence of 10 μM UCM–1341. The values represent the means±S.E.M. (n=5). One-way ANOVA with Bonferroni post hoc analysis. * $p < 0.05$ versus control. ^ $p < 0.05$ versus LPS+ IFN–γ. **D,** Quantitative analysis of resting + intermediate (dark blue), amoeboid (light blue), foamy (green), dystrophic (black) microglia phenotypes, in control, LPS+IFN-γ–treated, in the absence or in the presence of 10 μM UCM1341. Data were normalized to the total number of Iba^+ cells. The schematic diagram of microglia phenotypes is shown next to the graph. **E**; Quantitative analysis of foamy microglia/macrophages in control cultures, LPS+IFN-γ-treated, in the absence or in the presence of 10 μM UCM1341. The values represent the mean±S.E.M. (n=5). One-way ANOVA with Bonferroni post hoc analysis. * $p < 0.05$ versus control and LPS+IFN-γ.

Figure 8. Effect of UCM1341 on the expression of proteins controlling cholesterol metabolism and efflux. A-B. Western blot and quantitative densitometric analysis of TREM2 (A), LXR (B, *left*) and ABCA1 (B, *right*) levels in tissue lysates from control and LPS+IFN-γ-treated explants, in the absence or in the presence of 10 μM UCM1341. Data were normalized on the basis of β-actin levels and expressed as percentage of control. The values represent the mean±S.E.M. (n = 5). One-way ANOVA with Bonferroni post hoc analysis. * $p < 0.05$ versus control. **C,** Representative confocal

microscopic images showing Plin2 and Iba1 immunoreactivities in the CA1 hippocampal region under LPS+IFN-γ exposure, and LPS+IFN-γ + 10 μM UCM1341 for 72 hours. Scale bars in d-f, j-l: 20μm. Scale bars in a-c, g-i: 50μm. (m), Quantitative analysis of $Plin2^{+}/Iba1^{+}$ cells in control cultures, LPS+IFN-γ-treated, in the absence or in the presence of 10 μM UCM-1341. Panels d-f and j-l show high magnification images of squared areas in a and g, respectively. Data are expressed as percentage of the total $Iba1^{+}$ cells. The values represent the mean±S.E.M. (n = 5). Unpaired Student's t-test. * $p < 0.05$ versus LPS+IFN-γ. **D**, Representative confocal microscopic images showing ABCA1 and Iba1 immunoreactivities in the CA1 hippocampal region under LPS+IFN-γ exposure, and LPS+IFN-γ + 10 μM UCM1341 for 72 hours. Arrow in c-d point to cells with plasma membrane ABCA1 staining. Scale bar in a-d: 20 μm. Data are expressed as percentage of the total $Iba1^{+}$ cells. The values represent the means±S.E.M. (n = 5). Unpaired Student's t-test. * $p < 0.05$ versus LPS+IFN-γ.

Figure 9. Effect of UCM1341 on PPARα levels and of TRPV1, PPARα, and melatonin receptor antagonists on drug- induced neuroprotection

A, (a-l), PI fluorescence staining patterns observed in hippocampal slice cultures 96 hours following LPS+IFN-γ exposure in the absence (a) or in the presence of 10 μM UCM1341 (b), 0.1 μM AM251 alone or in combination with 10 μM UCM1341 (c-d), 0.1 μM AM630 alone or in combination with 10 μM UCM1341 (e-f), 30 nM SB3667 alone or in combination with 10 μM UCM1341 (g-h), 0.1μM GM6471 alone or in combination with 10 μM UCM1341 (i-j) and 0.1 μM luzindole alone or in combination with 10 μM UCM1341 (k-l) respectively; **B**, Quantitative densitometric analysis of PI fluorescence uptake recorded in slices under control conditions, and after LPS+IFN-γ, in the presence of 0.1 μM AM251, 0.1μM AM630, 30 nM SB3667, 10 μM GM6471 and 0.1 μM luzindole, alone or in combination with 10 μM UCM1341. Data are expressed as percentage of control. The values represent the mean±S.E.M. (n = 5). One-way ANOVA with Bonferroni post hoc analysis. *$p < 0.05$ versus UCM1341. **C**, Protein expression and quantitative densitometric analysis of PPARα in tissue lysates from control, LPS+IFN-γ-treated, in the absence or in the presence of 10 μM melatonin, 10 μM URB597, 10 μM UCM1341, 10 μM melatonin + 10 μM URB597. Data were normalized on the basis of β-actin levels and expressed as percentage of control. The values represent the mean ± S.E.M. (n = 5). One-way ANOVA with Bonferroni post hoc analysis. * $p < 0.05$ versus control.

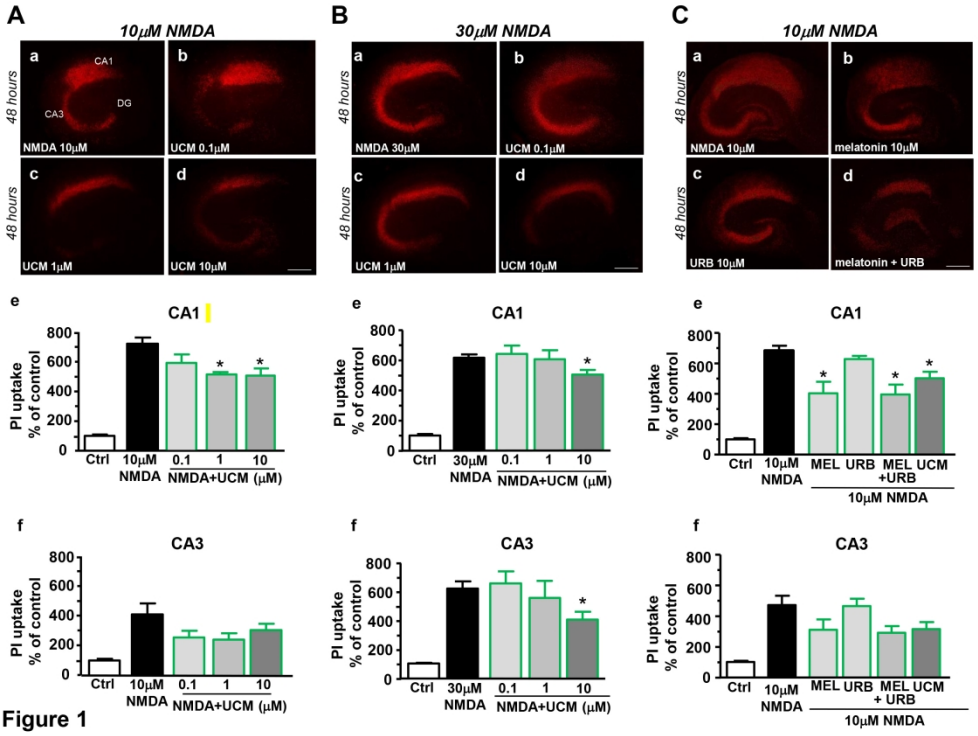

Figure 1

Figure 1/Figure 1. Dose-dependent effects of UCM1341 against NMDA-induced neurodegeneration in hippocampal explants. A-B, PI fluorescence staining patterns (a-d) and densitometric quantification of PI uptake in hippocampal CA1 and CA3 subfields (e-f) measured 48 hours following 10 μM NMDA (A) or 30 μM NMDA (B) exposure in the absence or in the presence of 0.1-10 μM UCM1341, respectively. Scale bars in a-d: 500 μm. C, PI fluorescence staining patterns (a-d) and densitometric quantification of PI uptake in hippocampal CA1 and CA3 subfields (e-f) measured 48 hours following 10 μM NMDA exposure in the absence or in the presence of 10 μM melatonin, 10 μM URB597, 10 μM melatonin + 10 μM URB597. Scale bars in a-d: 500 μm. Data are normalized as percentage of control. The values represent the mean±S.E.M (n = 5). One-way ANOVA with Bonferroni post hoc analysis. *p < 0.05 versus NMDA.

254x190mm (300 x 300 DPI)

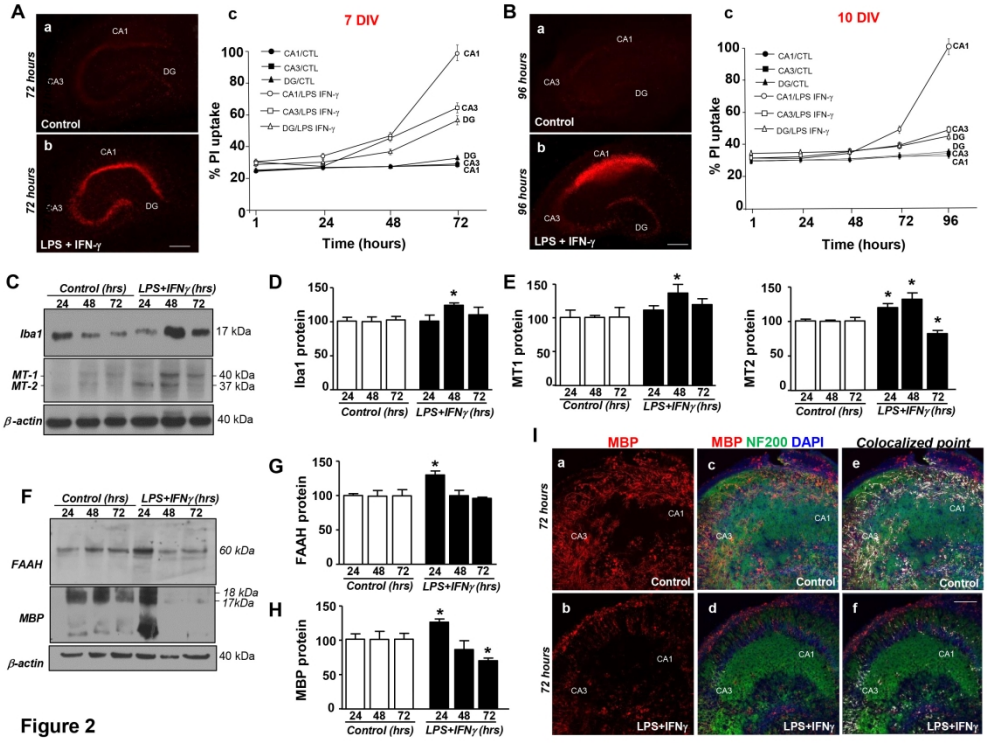

Figure 2

Figure 2/Figure 2. Time-dependent effects of LPS+IFN-γexposure on PI uptake, and Iba1, MBP, FAAH and melatonin receptor protein levels in rat hippocampal explants. A-B, Representative images (a-b) and quantitative densitometric analysis (c) of PI fluorescence uptake recorded in the CA and DG subfields of 7 DIV slices (A) or 10 DIV slices (B) exposed to LPS + IFN-γ for 72 or 96 hours, respectively. Data are expressed as percentage of the maximal value of PI fluorescence observed in the CA1 subregion upon 72 or 96 hours of LPS + IFN-γ exposure, respectively. Each data point is the mean±S.E.M. (n=5). Scale bars in a-b: 500 □m. C-E, Western blot (C) and quantification of Iba1 (D) and melatonin MT1/MT2 receptor (E) protein levels in hippocampal slices under control conditions and after LPS + IFN-γ exposure for 24-72 hours. Data were normalized on the basis of β-actin and expressed as percentage of controls. The values represent the mean±S.E.M. (n = 5). One-way ANOVA with Bonferroni post hoc analysis. *p < 0.05 versus respective control. F-H, Western blot (F) and quantification of FAAH (G) and MBP (H) protein levels in hippocampal slices under control conditions and after LPS + IFN-γ exposure for 24-72 hours. Data were normalized on the basis of β-actin and expressed as percentage of controls. The values represent the mean±S.E.M. (n = 5). One-way ANOVA with Bonferroni post hoc analysis. *p < 0.05 versus respective control. F, Representative confocal double immunofluorescence images displaying the distribution of MBP (red) and NF200 (green) immunoreactivities and their colocalization (white) in untreated (a, c, e) and LPS + IFN-γ-treated (b, d, f) slices for 72 hours. Scale bar in a-f: 200 μm.

254x190mm (300 x 300 DPI)

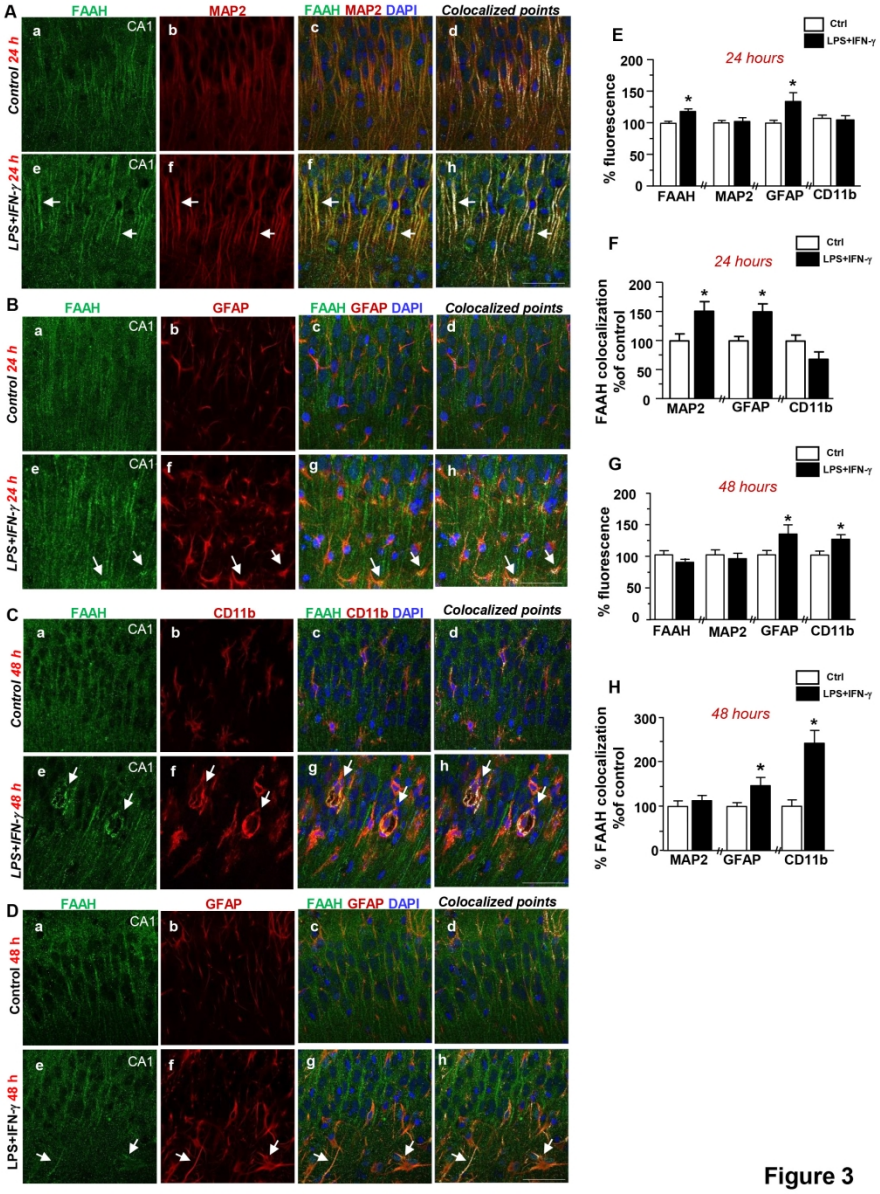

Figure 3

Figure 3/Figure 3. Distribution of FAAH immunoreactivity in neurons, astrocytes and microglia of hippocampal explants during LPS+IFN-γ exposure. A-B, Representative confocal images displaying the colocalization of FAAH with MAP2 (A) or FAAH with GFAP (B) immunoreactivities in the CA1 hippocampal region, in the absence (a–d) or in the presence of LPS + IFN-γ (e–h) for 24 hours. C-D, Confocal images displaying colocalization of FAAH with CD11b (C) or FAAH with GFAP (D) immunoreactivities in the CA1 hippocampal region, in the absence (a–d) or in the presence of LPS+IFN-γ (e–h) for 48 hours. In A-D, panels d and h display the colocalized points (white). Arrows in e-h point to colocalizing cells. Scale bars: 50μm. E-F, Quantitative analysis of FAAH, MAP2, GFAP, and CD11b immunofluorescence intensities (E) and FAAH colocalization with MAP2, GFAP, or CD11b immunosignals (F) in the CA1 hippocampal region, in the absence or in the presence of LPS+IFN-γ for 24 hours. G-H, Quantitative analysis of FAAH, MAP2, GFAP, and CD11b immunofluorescence intensities (G) and FAAH colocalization with MAP2, GFAP, and CD11b immunosignals (H) in the absence or in the presence of LPS+IFN-γ for 48 hours. Data were obtained from 5 microscope fields per slice in each group and expressed as percentage of control. The values represent the mean+S.E.M. (n=5). Unpaired Student's t-test. *p < 0.05 versus respective control.

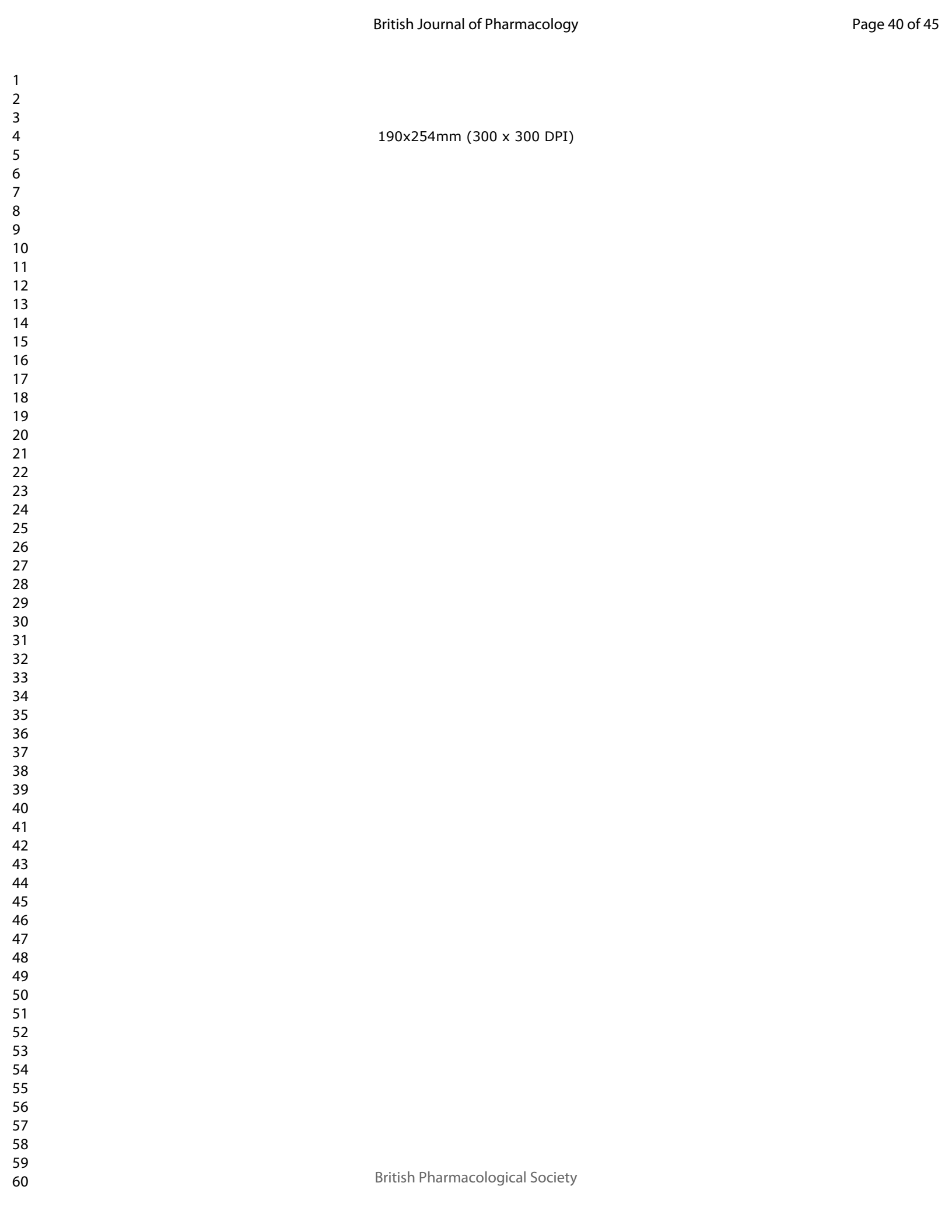
190x254mm (300 x 300 DPI)

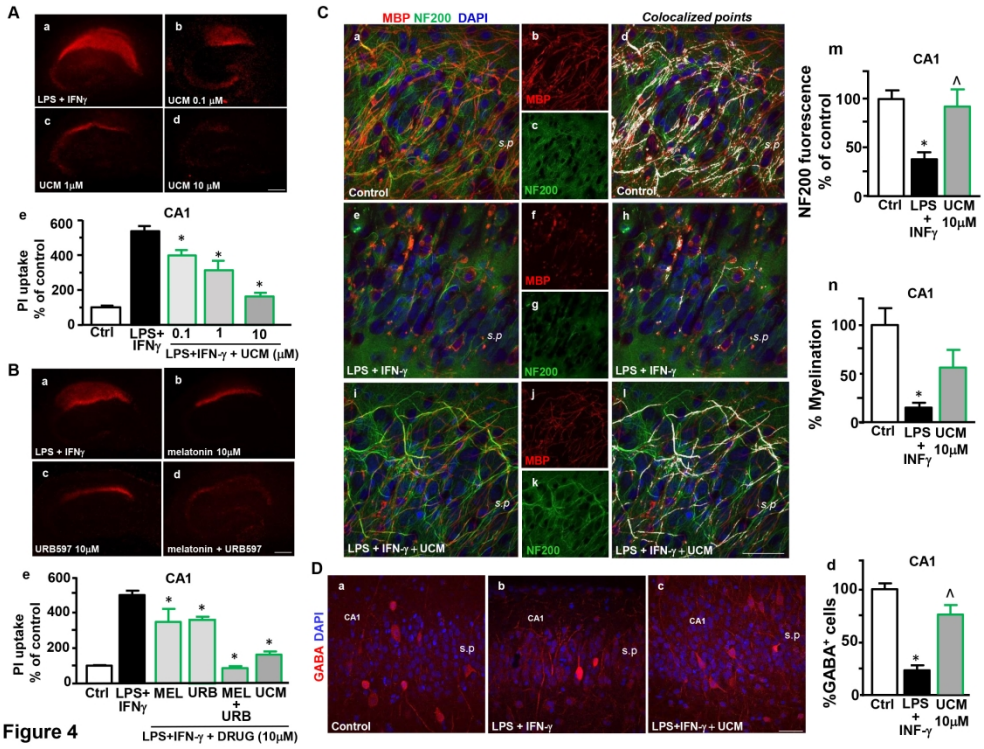

Figure 4

Figure 4/Figure 4. Protective effects of UCM1341 against neuroinflammation-induced degenerationA, PI fluorescence staining patterns (a-d) and quantitative densitometric analysis of PI uptake (e) in the CA1 region following LPS+IFN-γ exposure in the absence or in the presence of 0.1-10 μM UCM1341 for 96 hours. The values represent the mean+S.E.M. (n=5). One-way ANOVA with Bonferroni post hoc analysis. *p < 0.05 versus LPS+IFN-γ. B, PI fluorescence staining patterns (a-d) and quantitative densitometric analysis of PI uptake (e) in the CA1 region following LPS+IFN-γ exposure in the absence or in the presence of 10 μM melatonin, 10 μM URB597, 10 μM melatonin + 10 μM URB597, and 10 μM UCM1341 for 96 hours. The values represent the mean+S.E.M. (n=5). One-way ANOVA with Bonferroni post hoc analysis. *p < 0.05 versus LPS+IFN-γ. Scale bars in a-d: 500 μm. C, (a-c), Representative maximum intensity projection of z-stack confocal images displaying NF200 (green) and MBP (red) immunoreactivities in the CA1 region of 10 DIV hippocampal slices under control conditions (a-d), and LPS+IFN-γ exposure in the absence (e-h) or in the presence of 10 μM UCM1341 (i-l) for 96 hours. Panels d, h, and l display colocalized points (white). Scale bars in a-l: 50 μm. (m), Quantitative analysis of NF200 immunofluorescence intensity under control conditions and in the presence of LPS+IFN- γ and LPS+IFN-γ +10 μM UCM1341- The values represent the mean±S.E.M. (n=5). One-way ANOVA with Bonferroni post hoc analysis. *p < 0.05 versus control. ^p < 0.05 versus LPS+IFN-γ), Analysis of the myelination index in the pyramidal/oriens layers of the CA1 region in 10 DIV hippocampal slices under control conditions and following LPS + IFN-γ exposure in the absence or in the presence of UCM1341. The values represent the mean+S.E.M. (n=5). One-way ANOVA with Bonferroni post hoc analysis. *p < 0.05 versus control. D, Representative confocal images (a-c) and quantitative analysis of GABA-positive cells (d) in the pyramidal layer of the CA1 hippocampal region, under control conditions or following LPS + IFN-γ in the absence (b) or in the presence (c) of UCM1341 for 96 hours. Scale bars in a-c: 50 μm. The values represent the mean+S.E.M. (n=5). One-way ANOVA with Bonferroni post hoc analysis. *p < 0.05 versus control. ^p < 0.05 versus LPS+IFN-γ

254x190mm (300 x 300 DPI)

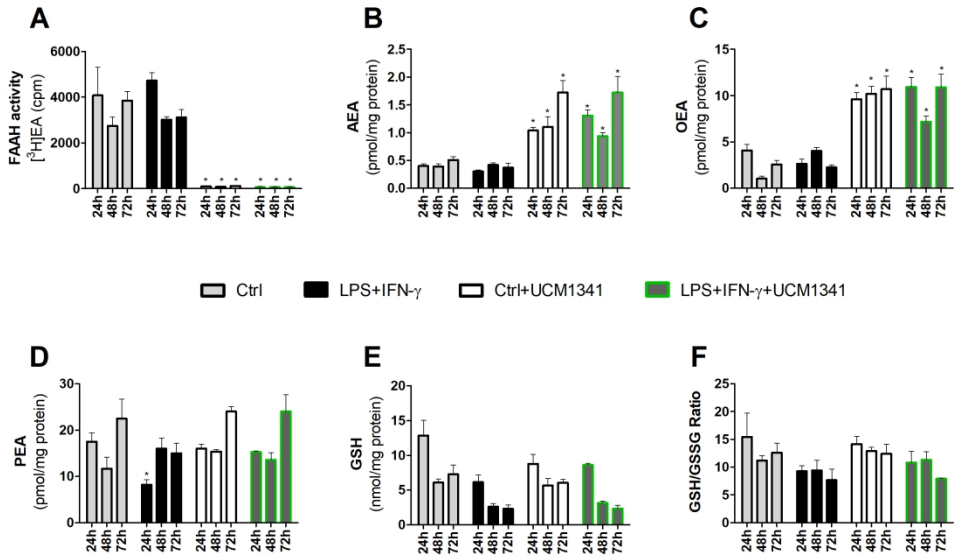

Figure 5/Figure 5. Effect of UCM1341 on FAAH activity, and glutathione levels in hippocampal cultures. Fatty acid amide hydrolase (FAAH) activity (panel A), anandamide (AEA, panel B), N-oleoylethanolamine (OEA, panel C), N-palmitoylethanolamine (PEA, panel D), reduced glutathione (GSH, panel E) levels and GSH/GSSG ratios in organotypic hippocampal slices under control conditions or after LPS+IFN-γ exposure in the absence or in the presence of 10 μM UCM1341 for 24-72 hours (Ctrl, light gray bars); LPS+IFN-γ (black bars); Ctrl+10 μM UCM1341 (white bars); LPS+IFN-γ+ 10 μM UCM1341 (green/gray bars). Results are expressed as mean value±S.E.M (n=5). One-way ANOVA with Bonferroni post hoc analysis. *p<0.05 if compared to corresponding control experiment.

248x146mm (300 x 300 DPI)

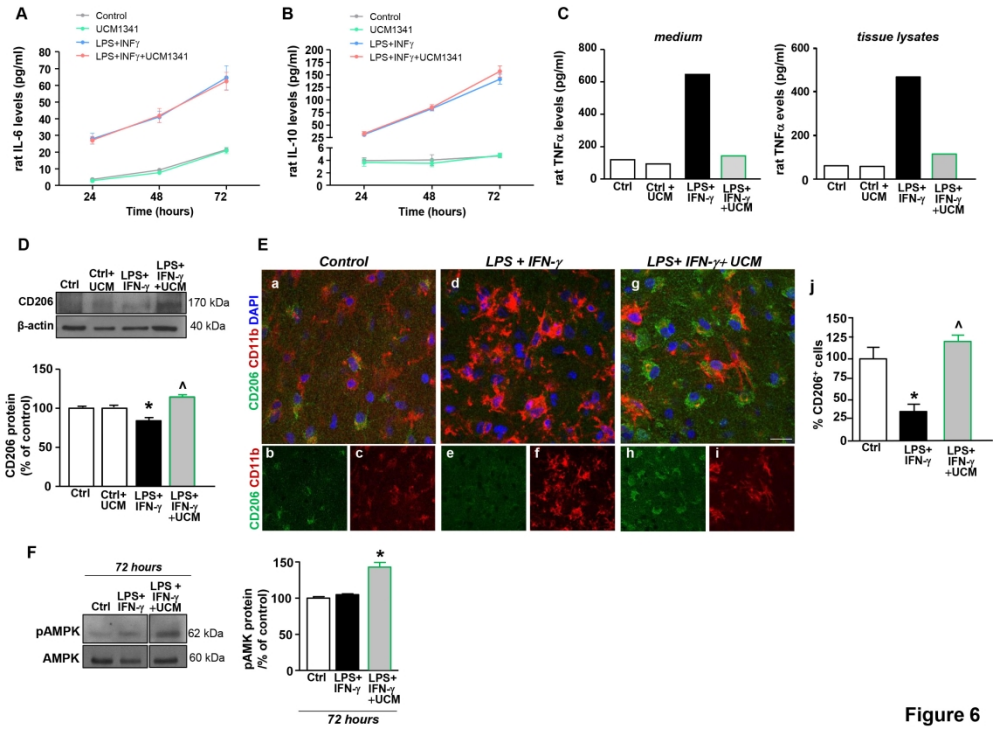

Figure 6

Figure 6/Figure 6. Effect of UCM1341 on TNF□□release, CD206 expression, and AMPK phosphorylation. A-B, Time-dependent production of IL-6 (A) and IL-10 (B) in the medium of explants cultures under control conditions or LPS+IFN-□ exposure in the absence or in the presence of 10 □M UCM1341 for 24-72 hours. Results are expressed as mean values ± S.E.M. (n=3). C, TNF□ determination in the medium (left) and tissue lysates (right) of hippocampal cultures under control conditions, and LPS+IFN-γ exposure in the absence or in the presence of 10 μM UCM1341 for 72 hours. Results are expressed as mean values ± S.E.M. Experiments were performed in duplicate. D, Western blot and densitometric analysis of CD206 protein levels in hippocampal lysates under control conditions and after LPS+ IFN-γ exposure in the absence or in the presence of 10 μM UCM1341 for 72 hours. Data were normalized on the basis of β-actin levels and expressed as percentage of control. The values represent the mean±S.E.M. (n = 5). One-way ANOVA with Bonferroni post hoc analysis. * $p < 0.05$ versus control. ^ $p < 0.05$ versus control and LPS+ IFN-γ E, (a-i), Representative confocal microscopic images showing CD206 and CD11b immunoreactivities in the CA1 hippocampal region under control conditions, LPS + IFN-γ exposure, and LPS+IFNγ + 10 μM UCM1341. Scale bar: 20μm E, (j), Quantitative analysis of CD206+ cells in slices under control conditions, and LPS+IFN-γ +LPS+IFN-γ + 10 μM UCM1341 exposure for 72 hours. Data are expressed as percentage of control. The values represent the mean±S.E.M. (n=5). One-way ANOVA with Bonferroni post hoc analysis.* $p < 0.05$ versus control. ^ $p < 0.05$ versus LPS+ IFN-γ. F, Western blot and densitometric analysis of pAMPK levels in hippocampal slices under control conditions and after LPS+IFN-γ exposure for 72 hours or in the presence of 10 γM UCM1341. Data were normalized on the basis of AMPK levels and expressed as percentage of control. The values represent the mean±S.E.M. (n = 5). One-way ANOVA with Bonferroni post hoc analysis. * $p < 0.05$ versus control and LPS+ IFN-γ.

254x190mm (300 x 300 DPI)

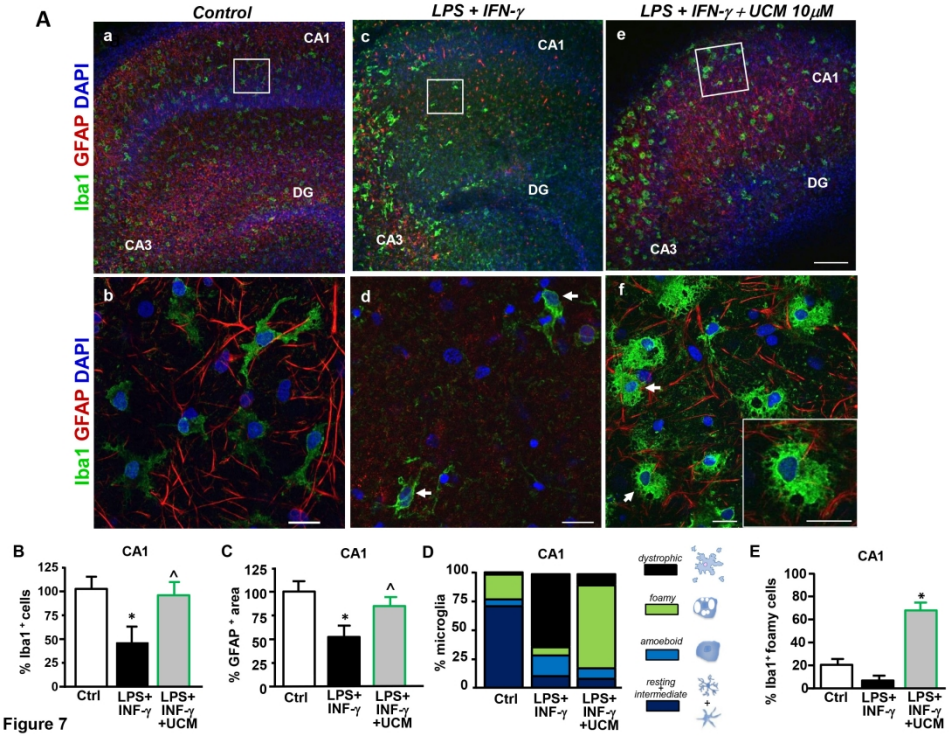

Figure 7

Figure 7/Figure 7. Effect of UCM1341 on microglia and astrocyte immunoreactivities following LPS+IFN-γ exposure. A, Representative confocal microscopic images showing Iba1 (green) and GFAP (red) immunoreactivities in the CA1 hippocampal region of cultures under control conditions and after LPS+IFN-γ exposure in the absence or in the presence of 10 μM UCM1341 for 96 hours. Panels b-f show higher magnification images of squared areas in a-c. Arrows in d and f point to dystrophic or foamy microglia/macrophages, respectively. Scale bars in a, c, e: 200 μM; in b, d, f: 20 □m. B-C, Quantitative analysis of Iba1+ cells (B) and GFAP+ area (C) in control cultures, LPS+IFN-γ treated cultures, in the absence or in the presence of 10 μM UCM1341. The values represent the means±S.E.M. (n=5). One-way ANOVA with Bonferroni post hoc analysis. * $p < 0.05$ versus control. ^ $p < 0.05$ versus LPS+ IFNγ D, Quantitative analysis of resting + intermediate (dark blue), amoeboid (light blue), foamy (green), dystrophic (black) microglia phenotypes, in control, LPS+IFN-γ□treated, in the absence or in the presence of 10 □M UCM1341. Data were normalized to the total number of Iba+ cells. The schematic diagram of microglia phenotypes is shown next to the graph. E; Quantitative analysis of foamy microglia/macrophages in control cultures, LPS+IFN-□-treated, in the absence or in the presence of 10 μM UCM1341. The values represent the mean±S.E.M. (n=5). One-way ANOVA with Bonferroni post hoc analysis. * $p < 0.05$ versus control and LPS+IFN-γ.

254x190mm (300 x 300 DPI)

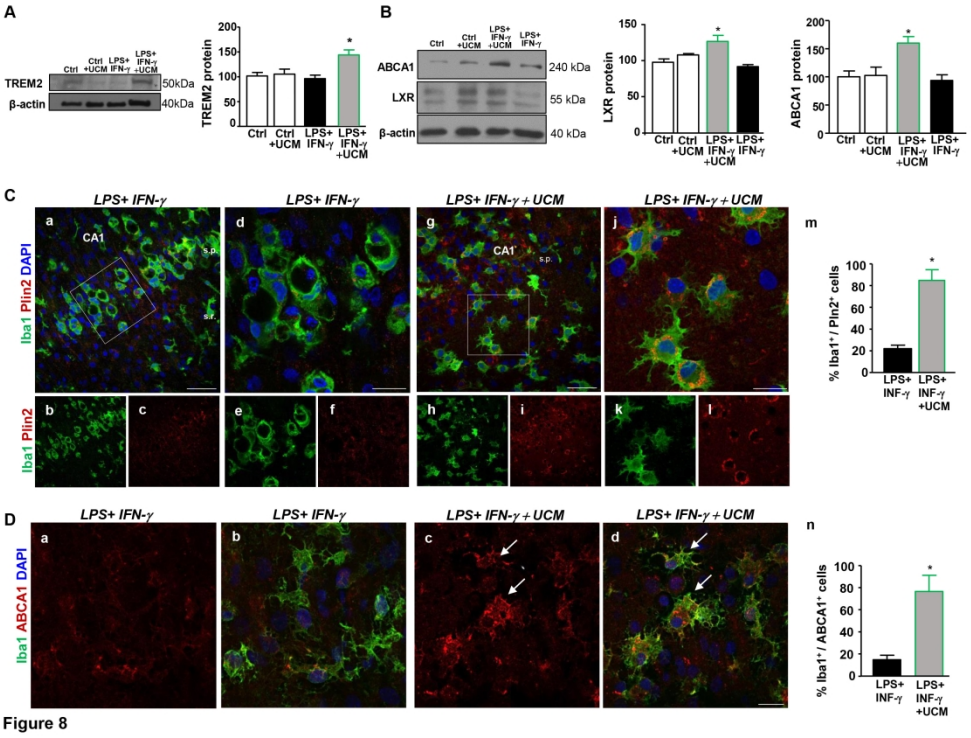

Figure 8

Figure 8/Figure 8. Effect of UCM1341 on the expression of proteins controlling cholesterol metabolism and efflux. A-B. Western blot and quantitative densitometric analysis of TREM2 (A), LXR (B, left) and ABCA1 (B, right) levels in tissue lysates from control and LPS+IFN-γ-treated explants, in the absence or in the presence of 10 μM UCM1341. Data were normalized on the basis of β-actin levels and expressed as percentage of control. The values represent the mean±S.E.M. (n = 5). One-way ANOVA with Bonferroni post hoc analysis. * $p < 0.05$ versus control. C, Representative confocal microscopic images showing Plin2 and Iba1 immunoreactivities in the CA1 hippocampal region under LPS+IFN-γ exposure, and LPS+IFN-γ + 10 μM UCM1341 for 72 hours. Scale bars in d-f, j-l: 20μm. Scale bars in a-c, g-i: 50μm. (m), Quantitative analysis of Plin2+/Iba1+ cells in control cultures, LPS+IFN-□-treated, in the absence or in the presence of 10 μM UCM-1341 Panels d-f and j-l show high magnification images of squared areas in a and g, respectively. Data are expressed as percentage of the total Iba1+ cells. The values represent the mean±S.E.M. (n = 5). Unpaired Student's t-test. * $p < 0.05$ versus LPS+IFN-□. D, Representative confocal microscopic images showing ABCA1 and Iba1 immunoreactivities in the CA1 hippocampal region under LPS+IFN-γ exposure, and LPS+IFN-γ + 10 μM UCM1341 for 72 hours. Arrow in c-d point to cells with plasma membrane ABCA1 staining. Scale bar in a-d: 20 μm. Data are expressed as percentage of the total Iba1+ cells. The values represent the means±S.E.M. (n = 5). Unpaired Student's t-test. * $p < 0.05$ versus LPS+IFN-γ.

254x190mm (300 x 300 DPI)

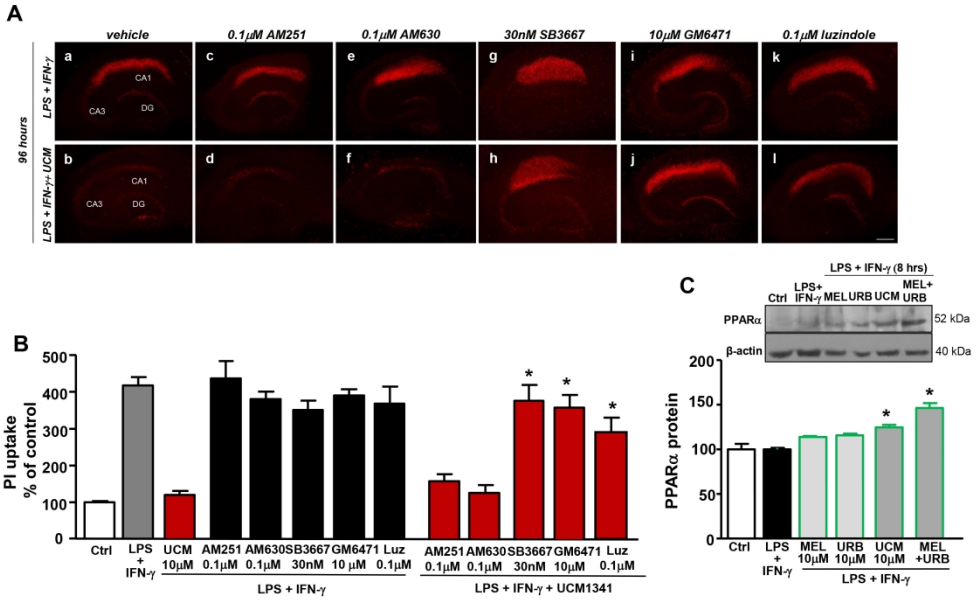

Figure 9

Figure 9/Figure 9. Effect of UCM1341 on PPARα levels and of TRPV1, PPARα, and melatonin receptor antagonists on drug- induced neuroprotection . A, (a-l), PI fluorescence staining patterns observed in hippocampal slice cultures 96 hours following LPS+IFN-γ exposure in the absence (a) or in the presence of 10 μM UCM1341 (b), 0.1 μM AM251 alone or in combination with 10 μM UCM1341 (c-d), 0.1 μM AM630 alone or in combination with 10 μM UCM1341 (e-f), 30 nM SB3667 alone or in combination with 10 μM UCM1341 (g-h), 0.1μM GM6471 alone or in combination with 10 μM UCM1341 (i-j) and 0.1 μM luzindole alone or in combination with 10 μM UCM1341 (k-l) respectively; B, Quantitative densitometric analysis of PI fluorescence uptake recorded in slices under control conditions, and after LPS+IFN-γ, in the presence of 0.1 μM AM251, 0.1μM AM630, 30 nM SB3667, 10 μM GM6471 and 0.1 μM luzindole, alone or in combination with 10 μM UCM1341. Data are expressed as percentage of control. The values represent the mean±S.E.M. (n = 5). One-way ANOVA with Bonferroni post hoc analysis. *p < 0.05 versus UCM1341. C, Protein expression and quantitative densitometric analysis of PPARα in tissue lysates from control, LPS+IFN-γ-treated, in the absence or in the presence of 10 μM melatonin, 10 μM URB597, 10 μM UCM1341, 10 μM melatonin + 10 μM URB597. Data were normalized on the basis of β-actin levels and expressed as percentage of control. The values represent the mean ± S.E.M. (n = 5). One-way ANOVA with Bonferroni post hoc analysis. * p < 0.05 versus control."

254x190mm (300 x 300 DPI)